photonics

MDPI

Review

Advancing Terahertz Biochemical Sensing: From Spectral Fingerprinting to Intelligent Detection

Haitao Zhang, Zijie Dai, Yunxia Ye * and Xudong Ren

School of Mechanical Engineering, Jiangsu University, Zhenjiang 212013, China;
2222303041@stmail.ujs.edu.cn (H.Z.); daizijie@ujs.edu.cn (Z.D.); renxd@ujs.edu.cn (X.R.)
* Correspondence: yeyunxia@ujs.edu.cn

Abstract

Biochemical detection is fundamental to various scientific disciplines, yet conventional methods still face inherent bottlenecks in achieving rapid, ultrasensitive, and simultaneous multi-target analysis. Terahertz (THz) waves, characterized by their unique spectral fingerprinting capabilities and non-destructive properties, have emerged as a compelling platform for advanced biochemical sensing. This review outlines the evolution of THz biochemical sensing over the past two decades, tracing its progression from passive identification toward intelligent perception. We structure this technological trajectory around four core themes: sensitivity enhancement, specific recognition, multi-target visualization, and system intelligence. We first evaluate the fundamental limitations of direct detection techniques, such as THz time-domain spectroscopy (THz-TDS). Building on this, we examine how metamaterial-assisted architectures utilize high-quality-factor resonances to achieve trace-level detection, pushing the limits of detection (LOD) down to the ng/mL or even pg/mL scale, and how surface chemical functionalization provides a molecular lock mechanism for selective targeting in complex samples. Furthermore, we highlight the paradigm shift from single-point spectral measurements to spatially resolved multi-target imaging using pixelated metasurfaces. Finally, the review addresses emerging directions, including dynamically tunable intelligent metasurfaces, multimodal on-chip integration platforms, and the growing integration of artificial intelligence (AI) in inverse design and data interpretation, which achieves classification accuracies exceeding 95% even in complex matrices. By synthesizing these developments, this review provides a comprehensive perspective on the future trajectory of THz sensing technologies.

Keywords: terahertz spectroscopy; metamaterials; biochemical sensing; fingerprint detection; intelligent sensing

Check for updates

Received: 22 March 2026
Revised: 3 April 2026
Accepted: 11 April 2026
Published: 16 April 2026

Copyright: © 2026 by the authors. Licensee MDPI, Basel, Switzerland. This article is an open access article distributed under the terms and conditions of the Creative Commons Attribution (CC BY) license.

1. Introduction

Terahertz waves are generally defined as electromagnetic radiation with frequencies ranging from 0.1 to 10 THz, bridging the gap between the microwave and infrared bands and exhibiting both electronic and photonic characteristics [1,2]. Owing to their low photon energy, high penetrative capability, and high sensitivity to molecular vibrational and rotational modes, THz technology has demonstrated significant potential in fields such as biomolecular fingerprint identification, non-destructive testing (NDT), and security imaging [3–10]. In the context of biochemical sensing, the THz band overlaps with the energy levels of hydrogen bonds and weak intermolecular interactions, providing a wealth of information for molecular recognition and structural elucidation. Its non-ionizing

nature ensures the integrity of biological specimens [11–14]. Despite these advantages, conventional THz techniques face inherent limitations when applied to clinical scenarios such as early-stage disease diagnosis. A primary obstacle is the large spatial mismatch between the sub-millimeter wavelengths of THz radiation and the nanometer-scale cross-sections of target biomolecules, which severely restricts detection sensitivity for trace-level analytes [15–17]. Additionally, the strong absorption of THz waves by aqueous environments, which are common in biological samples, poses a significant challenge to sensing accuracy [18]. This landscape of fundamentals and challenges is illustrated in Figure 1.

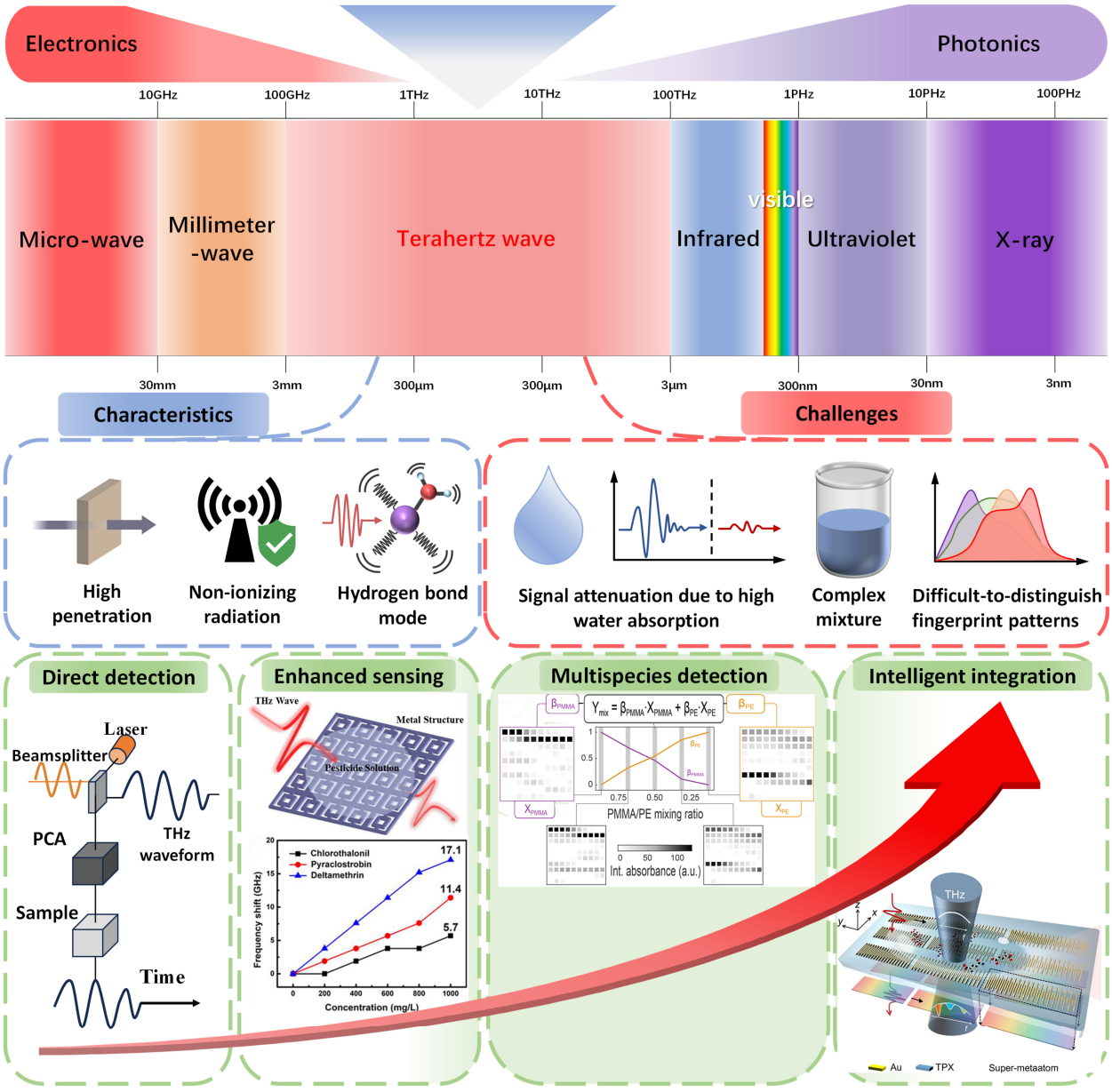

Figure 1. Fundamentals, challenges, and technological evolution of THz biochemical sensing.

In recent years, the emergence of metamaterials has provided a powerful approach for enhancing THz sensing performance [19,20]. As engineered composite structures, metamaterials enable unconventional electromagnetic responses, including negative refraction, perfect absorption, and electromagnetically induced transparency (EIT), through the precise design of subwavelength unit cells. These structures utilize localized field enhancement to amplify light-matter interactions at the microscale [21–23]. Compared to conventional bio-

chemical sensors, THz metamaterial-based platforms offer distinct advantages, including rapid response times, label-free operation, and minimal sample consumption [24].

Nevertheless, several critical hurdles remain. Detection sensitivities often fall short of the rigorous requirements for early clinical screening, specific recognition capabilities remain insufficient, and interference from aqueous absorption continues to be a major obstacle [25]. To circumvent these obstacles, various strategies have recently been proposed. For sensitivity enhancement, researchers have employed low-permittivity substrates, such as quartz, cyclic olefin copolymers, and polyimide, and engineered unit cells that support advanced resonance modes, including EIT, toroidal dipoles, and quasi-bound states in the continuum (quasi-BIC). Incorporating active materials like metallic nanoparticles or graphene has proven effective in further amplifying sensing signals [26]. Regarding specificity, functionalizing metamaterial surfaces with biorecognition elements, such as antibodies or aptamers, enables the selective capture of target molecules for precise qualitative analysis [27]. To mitigate water-induced interference, techniques including self-referencing reflection measurements, microfluidic integration, and hydrogel encapsulation have been explored. These approaches effectively suppress background noise while maintaining sample viability, thereby improving the practical application of THz sensing systems [28–30].

As the two-dimensional counterparts of metamaterials, metasurfaces have further expanded the functional integration of THz devices by enabling the flexible manipulation of wavefronts at the subwavelength scale [31–33]. By precisely tailoring the phase, amplitude, and polarization response of individual unit cells, metasurfaces can facilitate diverse functionalities, including beam steering, focusing, and holographic imaging, supporting the development of compact THz sensing systems [34–37]. However, conventional metasurfaces are inherently static; once fabricated, their electromagnetic responses are fixed, limiting their adaptability to complex and evolving detection environments. To address this, dynamically tunable metasurfaces have been developed. By incorporating responsive media such as liquid crystals, phase-change materials, or two-dimensional materials, and applying external stimuli, including electrical, thermal, optical, or mechanical triggers, these platforms achieve real-time modulation of THz amplitude, phase, and spectra. This progress enables reconfigurable sensing and imaging modalities [38–42]. As tunable and multifunctional metasurfaces become more complex, the challenges associated with their practical implementation intensify. Specifically, the discrepancy between manufacturing tolerances and idealized design performance has become a prominent issue for fabricated devices. To address these physical non-idealities, researchers are turning to digital strategies. Machine learning (ML) offers an effective approach to resolve these inconsistencies. Beyond its role in inverse design, performance prediction, and tolerance analysis, ML can implement back-end algorithmic compensation for device responses, thereby accelerating the integration of metasurfaces into practical sensing architectures [43–46].

To establish a clear framework for these rapid advancements, it is imperative to rigorously define the concept of intelligent sensing as utilized throughout this manuscript. Rather than a broad umbrella term, we conceptualize intelligent THz sensing as an integrated system architecture built upon three distinct but synergistic pillars: (1) Hardware Reconfigurability, which serves as the physical foundation where dynamically tunable metasurfaces adapt their electromagnetic responses to complex environments in real-time; (2) Algorithmic Intelligence, which acts as the computational core where artificial intelligence (AI) and ML execute structural inverse design, compensate for physical fabrication non-idealities, and extract latent high-dimensional target features from complex spectral data; and (3) System-Level Integration, which represents the operational architecture merging these active chips and AI models with automated microfluidics and multi-modal

platforms. Delineating these boundaries clarifies how isolated technological breakthroughs converge to form next-generation, sample-to-answer analytical systems.

In summary, terahertz biochemical sensing is advancing from fundamental spectroscopic analysis to metamaterial-enhanced sensing, and further toward multi-target visualization and intelligent integrated systems. This review outlines the key developments in this field, focusing on recent advancements in THz metamaterials and metasurfaces for enhancing detection sensitivity, specificity, and noise immunity. We further summarize recent progress in dynamic tuning strategies and intelligent design methodologies, and discuss future trends in interdisciplinary integration, smart devices, and high-fidelity biochemical monitoring.

2. Terahertz Detection Based on Spectral Fingerprinting

The physical foundation of terahertz detection lies in the resonant interactions between THz waves and the low-frequency vibrational, rotational, and lattice skeletal modes of molecules. This spectral window encompasses the energy scales associated with weak intermolecular forces, such as hydrogen bonding and van der Waals interactions. Consequently, various organic molecules, crystals, and biopolymers exhibit characteristic absorption features within this range, commonly referred to as fingerprint spectra, which provide the basis for substance identification [47]. THz-TDS operates by detecting the temporal response of a sample to femtosecond THz pulses. By performing a Fourier transform, both amplitude and phase information can be extracted, allowing for the simultaneous determination of the sample's absorption coefficient and refractive index for qualitative and quantitative analysis. However, a limitation of this technique is the scale mismatch. THz wavelengths in the sub-millimeter range are several orders of magnitude larger than target molecular dimensions at the nanometer scale, resulting in weak light-matter interactions and insufficient sensitivity [16]. To enhance the detection signal, early research primarily focused on optimizing experimental configurations. These efforts included employing high-resistivity silicon substrates to minimize dielectric losses, adjusting sample morphologies to extend the optical path length, and utilizing attenuated total reflection (ATR) modes to strengthen the evanescent field at the interface [22]. A schematic overview of the capabilities and inherent bottlenecks of traditional THz-TDS is presented in Figure 2.

In the analysis of solid-state samples, target analytes typically undergo pretreatment processes such as grinding, pelletizing, or solvent evaporation into thin films to form a dry, uniform layer, thereby eliminating water absorption interference. Integrating these samples with metamaterial structures can effectively amplify detection signals. For instance, Nie and colleagues utilized an all-dielectric broadband metamaterial absorber to detect forchlorfenuron pesticide in dried-film form, identifying a characteristic absorption peak at 1.33 THz with a limit of detection (LOD) of 0.1 mg/L, attributed to resonant field localization effects [48]. Similarly, Wang et al. performed quantitative analysis of tetracycline hydrochloride pellets using a multi-frequency resonant metamaterial, achieving an LOD of 0.1 ng at high-frequency resonance modes. This demonstrates that multimodal sensing improves quantitative reliability [49]. In a comparative study, Li and colleagues developed a graphene–metamaterial coupled sensor to distinguish various disease-related amino acids by analyzing spectral variances in the 1.2 to 1.8 THz range. They achieved an LOD of 10 ng/mL, enabled by the efficient capture and enrichment of target molecules through π-π stacking on the graphene surface [50]. Furthermore, Zhang et al. demonstrated enhanced sensitivity for detecting nadifloxacin-related pesticides using a metamaterial platform based on nitrogen-doped carbon nanotubes and gold nanoparticles [51]. In parallel, Du and colleagues investigated plant growth regulators, showing how structural variations in metamaterials directly influence spectral characteristics [52]. These studies

indicate that enhancing light-matter interaction through micro-nanostructure design or functional material hybridization improves THz fingerprint sensitivity. However, sensing performance remains dependent on the morphological compatibility between the sample and the sensing architecture.

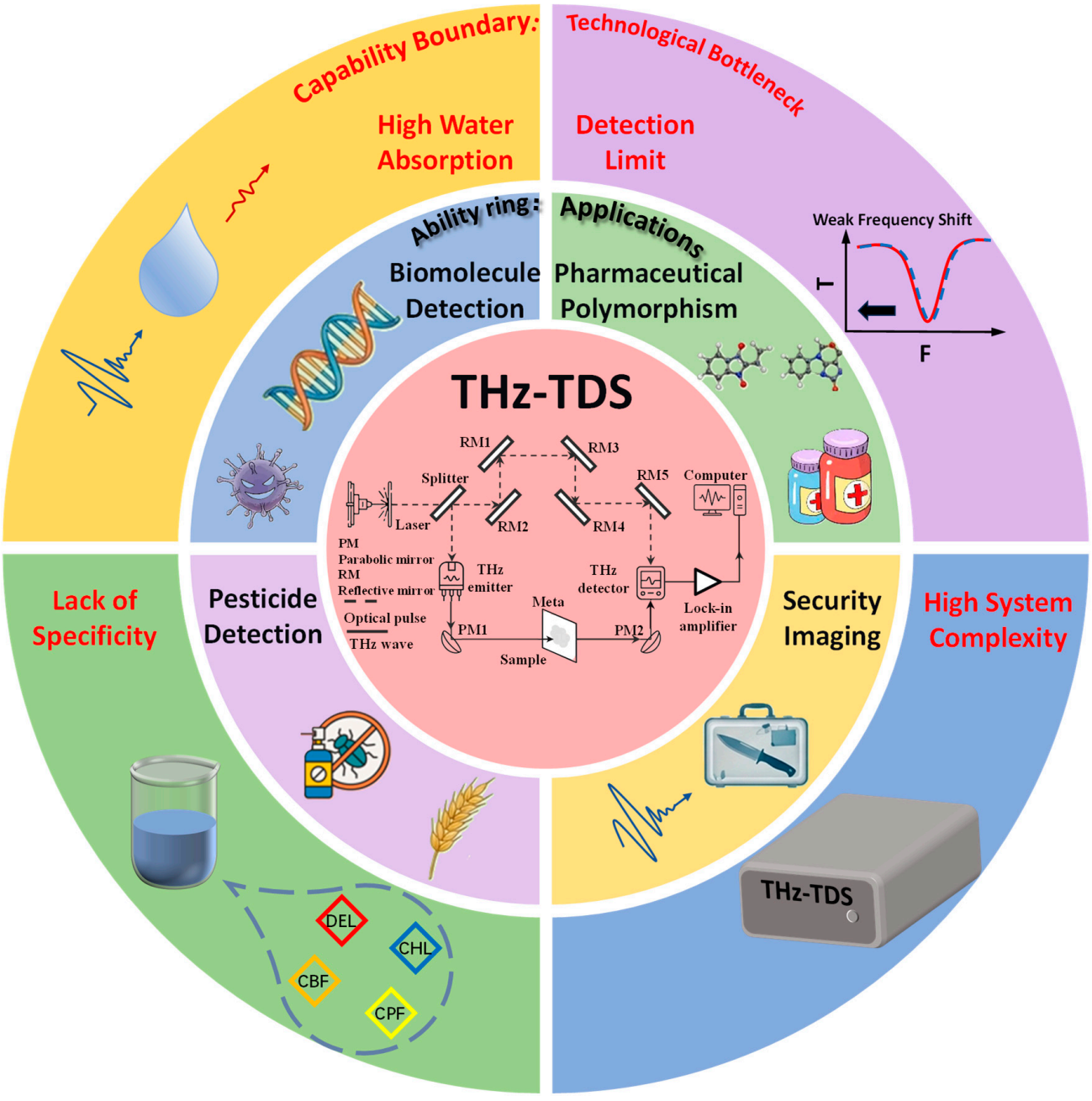

Figure 2. Capabilities and inherent bottlenecks of traditional THz-TDS.

The detection of liquid-phase samples, particularly aqueous solutions, remains the central challenge in this field due to the high absorption coefficient of water molecules in the THz regime [53]. To address this issue, researchers have explored strategies including microfluidic integration, ATR modes, and hydrogel encapsulation. Microfluidic technology mitigates water absorption by confining samples within microchannels of nanoliter to microliter volumes, shortening the THz interaction path length. For instance, Zhou and colleagues integrated a graphene–metamaterial architecture with a microfluidic chip to detect 100 nM DNA solutions. By minimizing the liquid layer thickness and utilizing near-

field enhancement, they maintained high sensitivity despite the aqueous environment [54]. Similarly, Geng et al. combined microfluidics with metamaterials for the trace detection of liver cancer biomarkers, demonstrating their application in complex liquid matrices [26].

The ATR mode uses the interaction between the evanescent field and the sample at a micrometer-scale depth, thereby avoiding bulk water absorption. Lee and colleagues applied this approach for glucose detection in serum. However, its sensitivity is often constrained by the lower intensity of the evanescent field compared to transmission-mode configurations [55]. Hydrogel encapsulation employs a hydrophilic three-dimensional network to immobilize biomolecules while displacing a portion of free water. This technique suppresses background interference while preserving biological activity. Zhou et al. achieved specific detection of thrombin in serum at 0.40 pM using an aptamer-functionalized hydrogel on a metamaterial surface [56]. The sensitivity of liquid-phase detection remains lower than that of solid-state systems, while requiring increased system complexity and fabrication expenses.

Although THz detection based on fingerprint spectra facilitates substance identification, it faces several limitations [57]. The sensitivity threshold is restricted by the spatial mismatch between THz wavelengths and molecular scales [2]. Despite enhancement techniques, current detection limits remain several orders of magnitude above the requirements for trace analysis, including single-molecule detection. Water absorption interference restricts aqueous-phase sensing, as current mitigation strategies compromise signal intensity or increase structural complexity [1]. The lack of specificity causes spectral overlapping of diverse constituents in complex matrices and increases susceptibility to environmental fluctuations, reducing identification reliability [58].

Beyond physical constraints, conventional THz-TDS systems require large equipment, such as femtosecond lasers, restricting their use in on-site rapid testing. Compact alternatives, including photoconductive antennas and quantum cascade lasers (QCLs) [59,60], are limited by bandwidth, stability, and cost. Integrating sample-handling technologies, such as microfluidics and stimuli-responsive hydrogels, with machine learning algorithms improves selectivity and resolution in complex systems. Monolithic on-chip integration of THz sources, detectors, and sensing platforms is necessary for practical applications.

3. Metamaterial-Enhanced High-Sensitivity Terahertz Sensing

Terahertz metamaterial sensing controls electromagnetic properties, including amplitude, phase, and polarization, through the arrangement of subwavelength unit cells. The enhancement mechanisms arise from spoof surface plasmon polaritons (SSPPs) and localized field resonances [19,20], illustrated in Figure 3a. SSPPs confine THz waves at the metal–dielectric interface, compressing the wavelength and increasing the surface electromagnetic field. When the dimensions of the unit cells are scaled to the THz regime, they excite localized resonances, such as toroidal dipoles (TDs) [61], electromagnetically induced transparency (EIT) [62], and quasi-bound states in the continuum (quasi-BIC) [63]. These modes concentrate incident energy into nanoscale regions, including structural gaps or edges. This localized field enhancement amplifies the electric field intensity by several orders of magnitude, magnifying the spectral response, such as resonance frequency shifts or transmittance variations, induced by perturbations in the analyte's dielectric environment. These mechanisms enable high-sensitivity sensing beyond the conventional diffraction limit.

Metamaterial sensing has progressed from utilizing fundamental resonances to optimizing quality factors and integrating functional dynamism. Early designs utilized conventional metallic and dielectric metamaterials [64], with unit cells such as split-ring resonators (SRRs) and rod antennas, relying on electric dipoles, LC circuits, or Fano res-

onance modes [65]. Although these sensors yield sensitivities between 100 and 200 GHz per refractive index unit (GHz/RIU), their performance is limited by ohmic and radiative losses in the metals, resulting in low quality factors (Q-factors) [66,67], as illustrated in Figure 3b. Subsequent research shifted toward high-Q resonance designs, particularly quasi-BIC. Quasi-BICs originate from bound states topologically protected by structural symmetry with infinite Q-factors. By introducing geometric asymmetries, such as dimensional perturbations, rotation, or symmetry breaking, the BIC couples to the radiative continuum, transforming into a quasi-BIC resonance with a high Q-factor [68,69]. Zhang and colleagues designed an asymmetric structure to break global symmetry [70], resulting in a THz angular sensor with a Q-factor of 120.6 and a sensitivity of 3.45 GHz per degree. Peng and colleagues designed a double C array metasurface to break structural symmetry [71], resulting in a quasi-BIC THz biosensor that achieves a 16-fold resonance amplitude enhancement and an ultra-sensitive limit of detection of 0.36 ng/mL, as shown in Figure 3c. Wang et al. developed an all-dielectric asymmetric tetramer cluster [72] achieving a toroidal dipole resonance with a Q-factor exceeding 2500. Its refractive index sensitivity reached 489 GHz/RIU, and its narrow linewidth enables the detection of trace-level biomolecules.

The third stage integrates materials that expand sensor functionality. All-dielectric metamaterials based on high-resistivity silicon eliminate metallic losses and achieve higher Q-factors. Two-dimensional materials such as graphene enable dynamic tuning of resonance frequencies through electrical gating of the Fermi level. Integrating phase-change materials, such as vanadium dioxide (VO_2), allows sensors to switch between functional states, acting as absorbers or filters under thermal, optical, or electrical stimuli. Liu and colleagues achieved localized field energy enhancement exceeding 400% and a sensitivity of 420 GHz/RIU in a hybrid metal-graphene structure by modulating the graphene Fermi level [73]. Tang et al. combined graphene with a Bragg reflector to excite robust resonance modes [74]. Optimizing the sensing medium thickness and graphene optical parameters yielded an angular sensitivity of 407.36 degrees per RIU, shown in Figure 3d. Figure 4a compares sensitivities across non-metamaterial sensors, metallic metamaterials, and quasi-BIC-based all-dielectric metamaterial sensors.

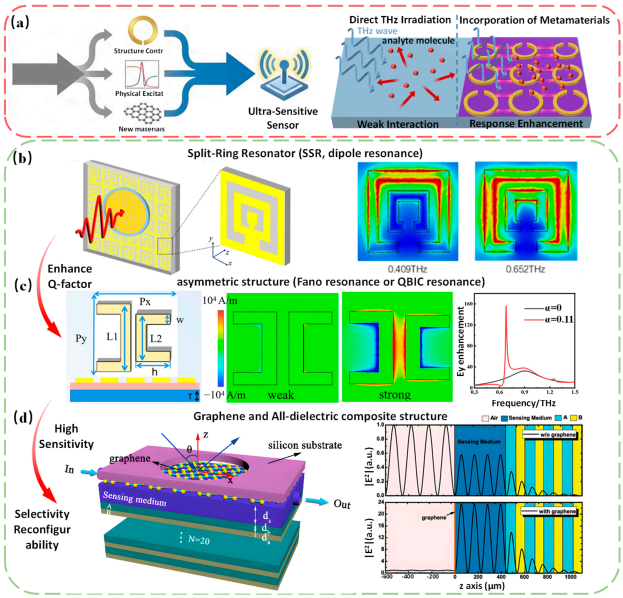

Figure 3. Metamaterial-enhanced mechanisms, structural evolution, and system-level integration for high-sensitivity THz sensing. (**a**) Schematic comparison of the enhancement principle between direct THz irradiation and metamaterial-enabled localized electric field confinement. (**b**–**d**) Structural evolution

of representative metamaterial unit cells and their electric field distributions. Reprinted from Ref. [67] Copyright 2025, The Author(s), Licensed under the Creative Commons Attribution CC BY 4.0. Reprinted from Ref. [71] Copyright 2024, The Author(s), Licensed under the Creative Commons Attribution CC BY 4.0. Reprinted from Ref. [74] Copyright 2024, The Author(s), Licensed under the Creative Commons Attribution CC BY 4.0.

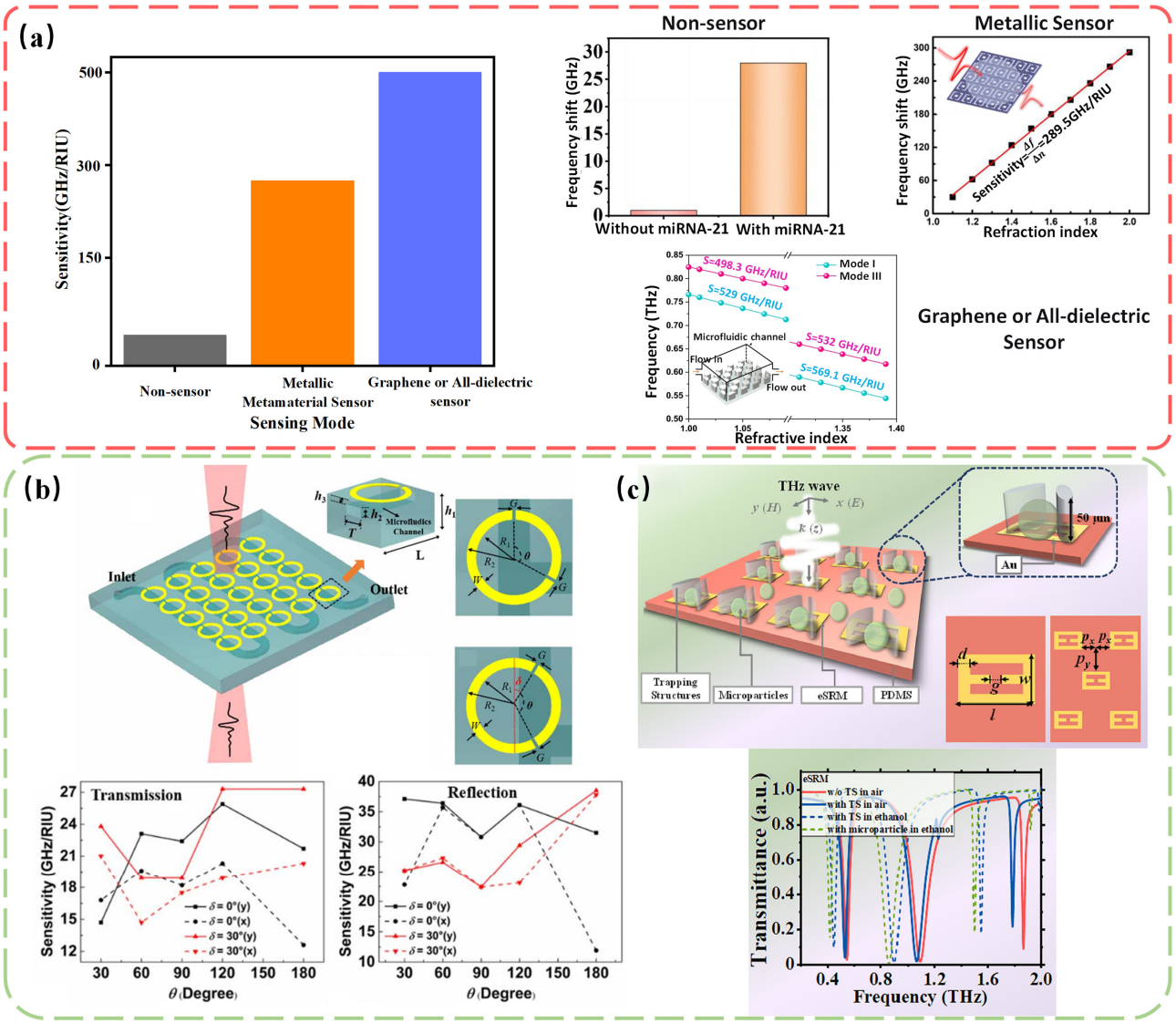

Figure 4. (**a**) Bar chart comparing the LOD across traditional THz-TDS, metallic metamaterials, and quasi-BIC all-dielectric sensors. Reprinted from Ref. [65] Copyright 2025, The Author(s), Licensed under the Creative Commons Attribution CC BY 4.0. Reprinted from Ref. [75] Copyright 2022, The Author(s), Licensed under the Creative Commons Attribution CC BY 4.0. Reprinted from Ref. [63] Copyright 2023 Optical Society of America under the terms of the OSA Open Access Publishing Agreement. (**b**) Schematic of embedding microchannels beneath the gaps of split-ring resonators to maximize liquid-sample interaction, positioning the aqueous analytes precisely within the maximum electric field hotspots. Reprinted from Ref. [65] Copyright 2022, The Author(s), Licensed under the Creative Commons Attribution CC BY 4.0. (**c**) A microfluidic-integrated perfect absorber sensor based on split-ring arrays. Reprinted from Ref. [65] Copyright 2022, The Author(s), Licensed under the Creative Commons Attribution CC BY 4.0.

To apply metamaterial sensitivity to liquid sensing, microfluidic integration and metamaterial absorber design serve as primary system-level strategies. Microfluidic technology transports and confines picolitre to nanoliter liquid analytes within specific regions of

the metamaterial. Subwavelength channel designs minimize the propagation loss of THz waves in aqueous solutions. Embedding microchannels into the metamaterial substrate or positioning them above the gaps of resonant units maximizes the spatial overlap between the sample and the electromagnetic fields. Li and colleagues demonstrated that embedding microchannels beneath the gaps of split-ring resonators allows the liquid sample to interact with the region of maximum electric field intensity [76], increasing interaction efficiency, illustrated in Figure 4b.

Metamaterial-based perfect absorbers provide a method for liquid-phase sensing. Matching the structural impedance with that of free space under critical coupling conditions achieves nearly 100% optical absorption at specific frequencies, confining incident energy within the metamaterial layer. These structures are highly sensitive to refractive index variations in the liquid on their surface. Xu and colleagues developed a microfluidic-integrated absorber sensor based on split-ring arrays [77], achieving a sensitivity of 523 GHz/RIU. This platform analyzed the particle size and concentration of suspended microparticles, illustrated in Figure 4c.

Although metamaterial enhancement improves THz sensing sensitivity, challenges limit practical applications. A primary issue is the lack of specificity. Metamaterials act as electromagnetic transducers. Their signal response reflects changes in the dielectric properties of the sensing region, lacking molecular recognition capabilities. Surface biofunctionalization, including the immobilization of antibodies, aptamers, or molecularly imprinted polymers (MIPs), provides selectivity. Introducing functional layers perturbs the electromagnetic field distribution, increases fabrication complexity, and prevents device reuse.

Current systems exhibit limited multi-target detection capabilities. Optimizing for a single analyte or resonance mode restricts the simultaneous detection of multiple analytes in biological matrices such as blood or interstitial fluid. Multiband resonators and spatially multiplexed arrays introduce design complexity, signal crosstalk, and data processing overhead. Developing metamaterials with high sensitivity and selectivity is necessary. Integrating these structures with microfluidics and artificial intelligence algorithms enables high-throughput, multi-target analysis in complex samples.

Table 1 summarizes the performance metrics of recently reported THz metamaterial sensors, comparing the Q-factors, sensitivities, and LOD across different sensing mechanisms. Cross-sectional analysis of these metrics reveals fundamental physical trade-offs among structural complexity, resonance quality, and sensing capability. Comparing absolute frequency shifts across different operational THz bands introduces inherent analytical bias. A normalized sensitivity metric, defined as the frequency shift relative to the fundamental resonance frequency (S/f_0), provides a standardized benchmark for evaluating structural efficacy independent of the operating spectrum. Symmetry-broken structures supporting quasi-BIC achieve Q-factors exceeding 100 [71]. This highly localized electromagnetic field confinement enables extremely low limits of detection suitable for trace analysis. The same confinement mechanism restricts the dynamic range, causing rapid spectral saturation at higher analyte concentrations. Metamaterial arrays relying on conventional dipolar or broadband plasmonic resonances exhibit lower intrinsic Q-factors but demonstrate wider dynamic ranges and higher tolerance to non-uniform analyte deposition. The selection of a specific metamaterial architecture is dictated by application constraints. Trace target detection in uniform environments necessitates high-Q designs. Bulk complex matrix analysis favors lower-Q structures with extended dynamic ranges to mitigate saturation and deposition irregularities.

Table 1. Performance metrics of reported THz metamaterial sensors.

Reference	Sensing Mechanism	Q-Factor	Sensitivity	LOD
[48]	Resonant field localization	-	-	100 ng/mL
[50]	PIT & π-π stacking	-	-	10 ng/mL
[78]	Antibody-functionalized resonance	-	-	24 pg/mL
[64–67]	LC circuits & dipole resonances	<30	100–200 GHz/RIU	-
[73]	Quasi-BIC	503	420 GHz/RIU	-
[72]	Toroidal dipole resonance	>2500	489 GHz/RIU	-
[77]	Perfect absorption	-	523 GHz/RIU	-

4. Functionalization Strategies for Specificity and Multiplexed Recognition

Functionalization strategies provide selective recognition and multiplexed detection for THz metamaterial sensors [79]. These strategies transduce biological recognition events or molecular vibrations into THz optical responses. Approaches have shifted from exogenous biochemical modifications to physical matching and from individual to multiplexed analysis. Current methods include constructing molecular locks at the sensing interface for specific capture, pretreating analytes for signal amplification, and utilizing spectrally selective physical enhancement based on resonance matching.

Surface functionalization provides molecular recognition capabilities through the chemical immobilization of biorecognition elements, such as antibodies and aptamers, or functional materials like graphene. Antibody-based functionalization relies on specific antigen-binding sites. Silanization typically achieves this immobilization. Ahmadivand and colleagues functionalized a plasmonic toroidal metamaterial with Zika virus antibodies [78], detecting viral envelope proteins with a LOD of 24 pg/mL. The sensing mechanism depends on the resonance frequency shift induced by local refractive index variations during antigen–antibody binding. Liu et al. modified a metasurface with halloysite nanotubes (HNTs) [80] to detect squamous cell carcinoma antigen (SCCA), illustrated in Figure 5a.

Aptamers provide chemical stability, broad target compatibility, and easy synthetic modification. Zhang and colleagues developed a metamaterial sensor based on a functionalized hydrogel network [81]. Embedding recognition units such as glucose oxidase within the hydrogel matrix enabled the detection of glucose in solutions, serum, and sweat. Graphene supports functionalization through its large specific surface area and π-electron cloud. These properties facilitate the adsorption of target molecules containing aromatic rings through non-covalent interactions, such as π-π stacking. Xu et al. constructed a graphene–THz metamaterial heterojunction [82], utilizing π-π interactions between graphene and the organophosphorus pesticide chlorpyrifos-methyl. This platform achieved specific adsorption of trace pesticides with a lower LOD than graphene-free structures.

Analyte pretreatment and signal amplification strategies target trace-level analysis, where direct analyte interaction yields negligible signals. Gold nanoparticles (AuNPs) enhance signals due to their high dielectric constant and easy functionalization. AuNPs modified with ligands, such as antibodies or aptamers, bind to target analytes and aggregate within sensing hotspots. This aggregation induces a localized refractive index change, magnifying resonance frequency shifts or amplitude variations. Yang and colleagues coupled antibody-modified AuNPs with a metamaterial [24], achieving an attomolar (aM) detection limit for microRNA-21.

Beyond acting as mass tags, functionalized AuNPs provide scaffolds for immobilizing capture antibodies at the sensing interface, improving sensitivity and specificity. Shi et al. modified an all-dielectric metasurface with AuNPs functionalized with anti-HA tag anti-

bodies to detect the HA antigen [83]. This configuration enhanced sensitivity to the HA antigen by a factor of 2.66 compared to bare metasurfaces. It distinguished the HA antigen from backgrounds containing bovine serum albumin (BSA), ovalbumin (OVA), and whey protein (WP), illustrated in Figure 5b.

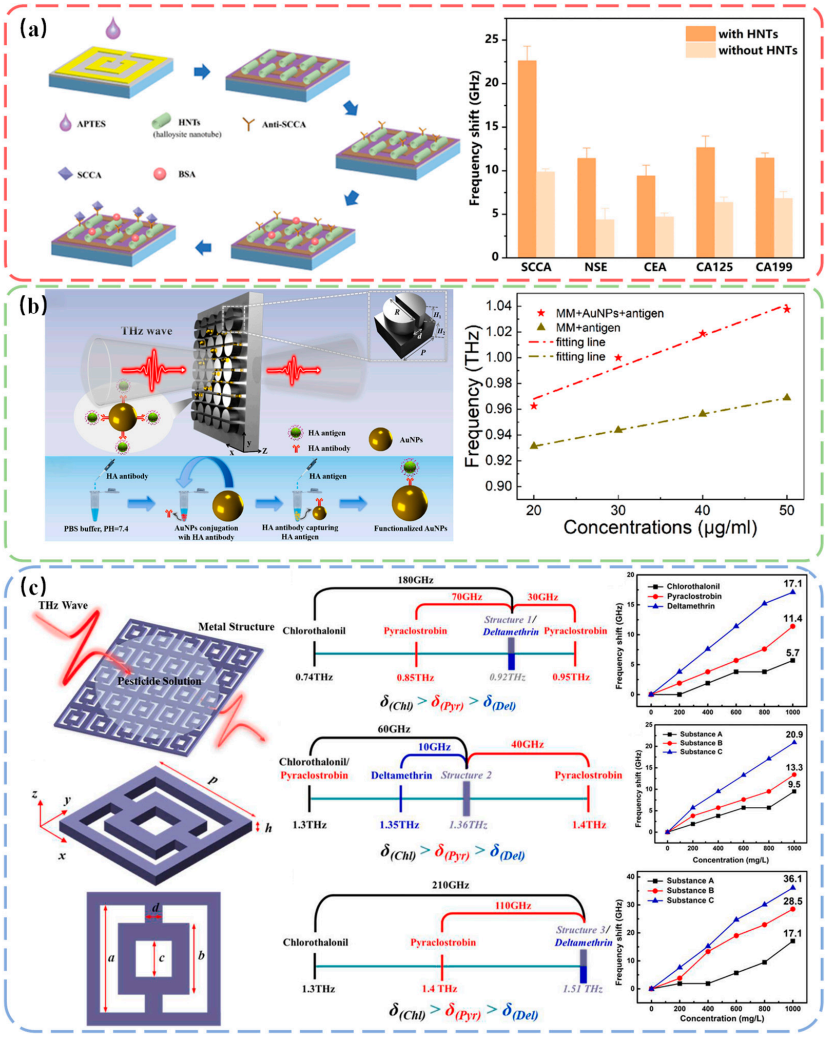

Figure 5. Functionalization strategies for specific recognition and signal amplification in THz sensing. (**a**) Schematic of a metamaterial unit cell modified with dense aptamers or antibodies to capture specific target molecules, enabling enhanced specific detection. Reprinted from Ref. [65] Copyright 2022, The Author(s), Licensed under the Creative Commons Attribution CC BY 4.0. (**b**) Analyte pre-treatment utilizing gold nanoparticle (AuNP)-labeled probes and strand displacement amplification (SDA) for target molecules (e.g., miRNA), generating massive complexes that cause a significant signal shift, effectively distinguishing trace-specific targets from complex background proteins. Reprinted from Ref. [65] Copyright 2022, The Author(s), Licensed under the Creative Commons Attribution CC BY 4.0. (**c**) Specificity enhancement based on resonance matching (the HIT effect), where the metamaterial's resonant peak is designed to match or approximate the intrinsic frequency of the analyte to amplify its specific response, allowing the definitive identification of unknown analytes via inverse peak inference. Reprinted from Ref. [75] Copyright 2022, The Author(s), Licensed under the Creative Commons Attribution CC BY 4.0.

Integrating isothermal nucleic acid amplification techniques, such as strand displacement amplification (SDA) or rolling circle amplification (RCA), converts a single target nucleic acid molecule into tandem repeats. These repeats tether signal tags, such as AuNPs, to the sensor surface, exponentially amplifying the signal. Niu and colleagues developed a sandwich immunosensor for carcinoembryonic antigen (CEA) using a toroidal dipole meta-

material [84]. Target protein capture and subsequent amplification with AuNPs labeled with secondary antibodies detected CEA at ng/mL concentrations.

Resonance-matching-based specificity relies on hybridization-induced transparency (HIT) or absorption-induced transparency (AIT) [85]. This phenomenon occurs when molecular vibrational frequencies couple with localized resonance modes, such as surface plasmon resonance, creating a sharp transparency window within a broadband absorption background. Weis and colleagues experimentally observed AIT signatures during the coupling of split-ring resonators with α-lactose molecules at 0.53 THz [86]. Zhao et al. identified specific substances by correlating molecular fingerprints with resonance frequency shifts (Δf) [75], as illustrated in Figure 5c. They fabricated three metallic-grid sensors using picosecond laser direct writing, tuning each to the fingerprint peaks of chlorothalonil, pyraclostrobin, and deltamethrin. The frequency deviation (δ), between the sensor resonance and the analyte fingerprint determines the magnitude of Δf at a given concentration. Smaller δ values yield stronger coupling and larger Δf. Comparing Δf sequences across different samples allows researchers to inversely infer fingerprint peak positions, achieving definitive identification of unknown pesticides.

Translating functionalized THz sensors to clinical settings encounters critical challenges regarding interfacial stability and electromagnetic interference. Biochemical receptors, particularly antibodies and aptamers, are susceptible to structural degradation and conformational changes over time, compromising long-term sensor stability and batch-to-batch reproducibility. In complex clinical matrices like whole blood or serum, the non-specific binding of background proteins competes with target recognition, severely degrading analytical specificity. The introduction of dielectric functionalization layers and bulky biological targets fundamentally alters the local electromagnetic environment. These adlayers often induce parasitic absorption and scattering, leading to the damping of metamaterial resonances and a corresponding reduction in the Q-factor [87]. This resonance broadening causes baseline shift instability, complicating the accurate extraction of resonant frequency variations and deteriorating the overall limit of detection. Overcoming these barriers requires the development of ultrathin, low-loss functional interfaces that maintain biological activity without compromising the structural quality factor. Resonance-matching strategies provide a label-free alternative but require stringent fabrication tolerances and depend on precharacterized THz fingerprint peaks in the target analytes.

Parallel analysis for high-throughput applications remains limited. Engineering sensor arrays or multimodal resonators for multi-target detection introduces cross-reactivity between recognition sites, microfluidic integration challenges, and computational complexity in interpreting multidimensional datasets. Functionalized platforms often exhibit poor reusability and lack the long-term stability data required for clinical evaluation.

Future progress requires stabilized, patternable, and universal functionalization interfaces. Integrating sensors with automated microfluidics enables complete sample analysis workflows. AI automates sensor inverse design, deconvolutes overlapping spectral signatures, and extracts latent features from high-dimensional data. These advancements translate laboratory prototypes into practical analytical systems.

5. Towards Simultaneous Multiplexed Detection and Spatial Chemical Visualization

Functionalization strategies improve specific target recognition but cannot simultaneously analyze multiple components or map chemical spatial distributions. Acquiring multidimensional information requires THz metamaterials to advance from discrete point measurements to continuous surface detection. This chapter examines simultaneous multi-target identification and chemical spatial distribution visualization. Sensor array strategies,

spectral spatial mapping mechanisms, and integrated THz imaging technologies enable high-throughput multi-component sensing.

Single-resonance metamaterial sensors struggle to identify specific targets within complex mixtures containing multiple analytes. Sensor arrays and pixelated platforms address this limitation. Integrating unit structures with distinct resonant frequencies or tailored surface functionalization creates optically addressable arrays. This parallel response capability enables simultaneous multi-target detection.

All-dielectric metasurfaces offer low intrinsic losses and high quality factors. Zhong et al. developed tilted silicon nanopillar arrays supporting high-Q quasi-BIC resonances [88]. This architecture identifies characteristic absorption peaks of tyrosine at 0.97 THz and santonin at 0.625 THz, shown in Figure 6a. Integrating diverse structural or functional units enables multi-component identification. Kawase et al. mapped the spatial distributions of methamphetamine and MDMA using multispectral THz transmission images, distinguishing them from aspirin within sealed envelopes [89]. Ye et al. developed a 2 × 2 sensor array combining three spoke-like metamaterial units (MM1, MM2, and MM3) with varying resonant frequencies [90], shown in Figure 7b. This array maps resonance frequency shifts (Δf) induced by analytes like chlorothalonil and deltamethrin into spatial intensity distributions within THz transmission images. Spectral overlap between each unit's resonance and the analyte fingerprint translates spectral responses into image contrast, allowing visual discrimination without complex spectral deconvolution.

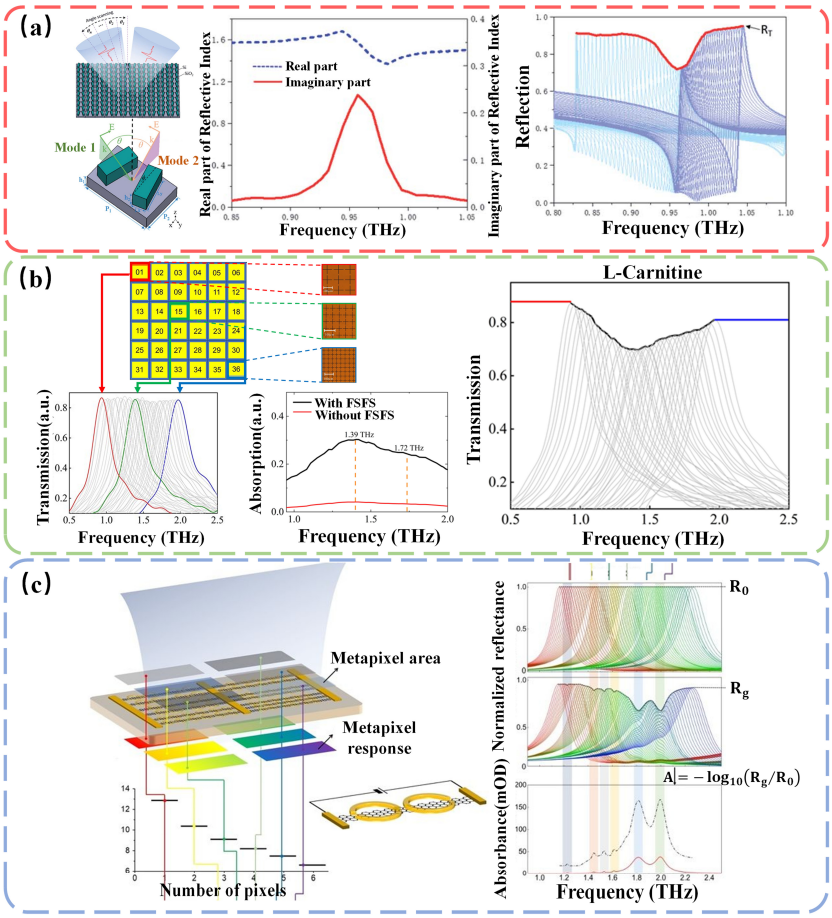

Figure 6. Transition from discrete point-based sensing to multi-target spatial visualization and multiplexed imaging. (**a**) All-dielectric metasurface based on tilted silicon nanopillar arrays (quasi-BIC) for the specific identification of distinct substances like tyrosine and santonin. Reprinted from Ref. [88] Copyright 2020, The Author(s), Licensed under the Creative Commons Attribution CC BY 3.0.

(**b**) Frequency-scanning fingerprint sensing (FSFS) platform for amplifying the signals of trace chiral enantiomers via the AIT effect. Reprinted from Ref. [12] Copyright 2023, The Author(s), Licensed under the Creative Commons Attribution CC BY 4.0. (**c**) Metasurface pixels integrating C-shaped resonators with tunable graphene microstrips to achieve one-to-many spatiospectral mapping, significantly expanding the information density of a single hardware pixel. Reprinted from Ref. [91] 2022 Used with permission of Royal Society of Chemistry, permission conveyed through Copyright Clearance Center, Inc.

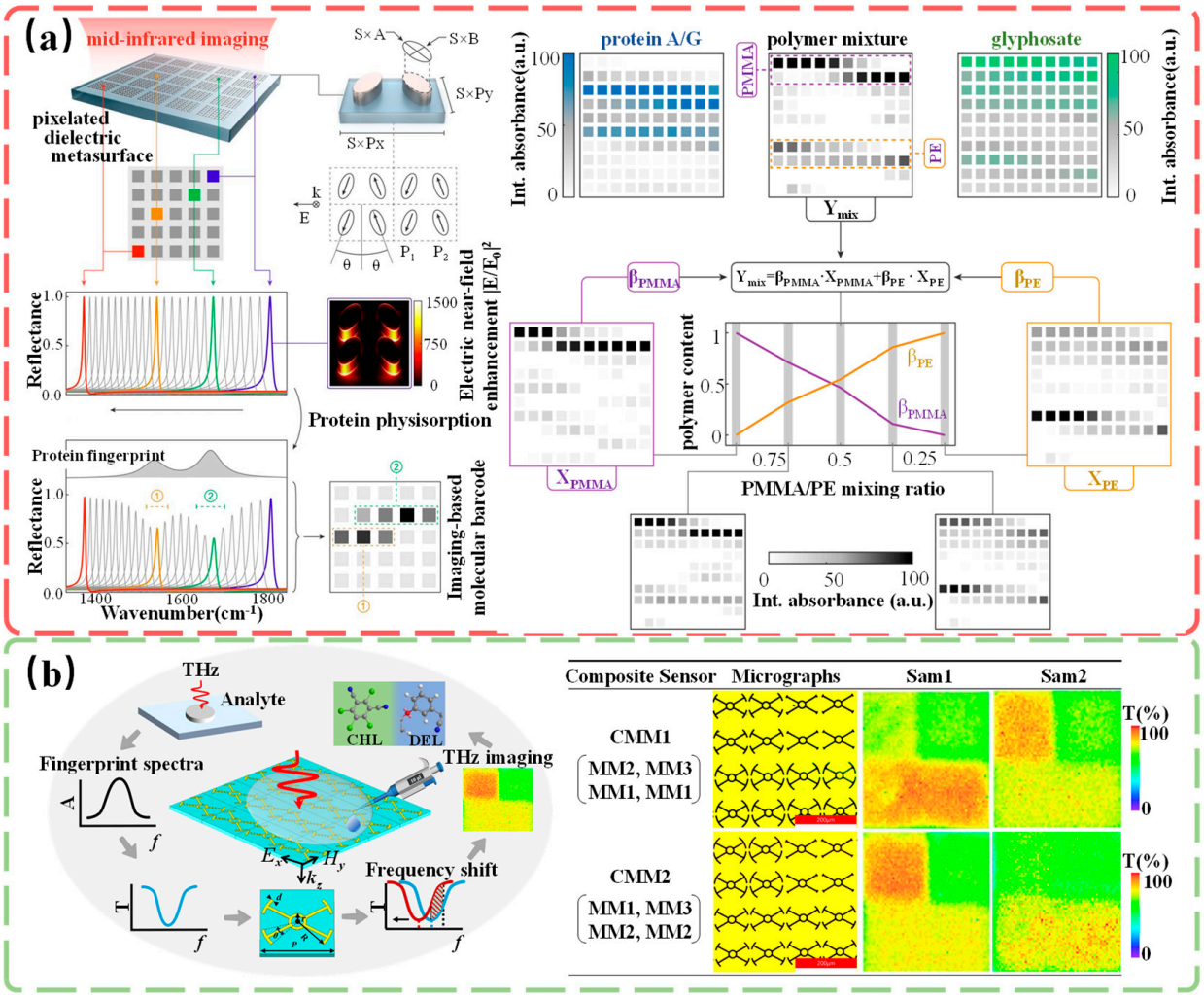

Figure 7. (**a**) Concept of imaging-based molecular barcoding that encodes one-dimensional spectral features into two-dimensional spatial distributions. Reprinted from Ref. [92] Copyright 2025, The Author(s), Licensed under the Creative Commons Attribution CC BY 4.0. (**b**) A two-by-two composite sensor array utilizing distinct spoke-like metamaterial units to translate the spectral responses of different analytes into characteristic spatial intensity images, enabling direct visual discrimination without complex spectral deconvolution. Reprinted from Ref. [90] Copyright 2026, The Author(s), Licensed under the Creative Commons Attribution CC BY 4.0.

Fu et al. introduced information metamaterials and programmable metasurfaces [93]. Integrating tunable media, such as graphene, liquid crystals, or micro-electro-mechanical systems (MEMS) actuators, enables dynamic control over the electromagnetic phase and amplitude of metasurface units. This control facilitates real-time functional reconfiguration and adaptive multi-target detection, matching a single hardware platform to diverse analyte fingerprints. Lyu et al. designed a frequency-scanning fingerprint sensing (FSFS) platform to enhance fingerprint signals of trace chiral enantiomers [12]. This platform amplified the molecular fingerprint signals of trace chiral carnitine between 0.95 and 2.0 THz by 8.65 dB,

shown in Figure 6b. Triggering the AIT effect in adjacent pixel groups facilitates broadband spectral analysis. They proposed a dual-degree-of-freedom multiplexing mechanism using angular and thickness multiplexing. However, the refractive index discrepancy between the microchannel fluid and the substrate limits its practical implementation.

Mapping spectral information onto spatial imagery enhances the visual characterization of chemical compositions. Following the mid-infrared molecular barcoding technique by Tittl et al. [94], shown in Figure 7a, THz researchers encode one-dimensional spectral features into two-dimensional spatial distributions. Pixelated metasurface platforms assign specific frequency selectivity to individual units. Analyte interaction generates unique absorption or transmission spatial patterns, establishing a spectrum to image correspondence. Watts et al. combined a reconfigurable metasurface spatial light modulator with compressive sensing algorithms to achieve single-pixel THz imaging [95]. This method reconstructs spatial and spectral information by switching metasurface coding patterns and collecting minimal projection data, bypassing point-by-point scanning for high-speed multispectral imaging. Sun et al. designed metasurface pixels covering the target THz fingerprint range by integrating symmetric metallic C-shaped resonators with tunable graphene microstrips [91]. This architecture achieves a one-to-many mapping between a single metasurface pixel and multiple characteristic absorption spectra, illustrated in Figure 6c, increasing the information density of the sensing platform.

Integrating THz metamaterial imaging technology advances discrete parameter measurement to real-space distribution visualization. Kuznetsov et al. constructed a multispectral THz imager using a pixelated metasurface absorber array with diverse absorption frequencies (0.30, 0.33, and 0.36 THz) and polarization sensitivities [96]. Converting incident THz energy into heat, captured by an infrared detector as thermal radiation, enables real-time uncooled imaging. Escobedia et al. monolithically integrated metamaterial absorbers with CMOS-processed PN diodes, creating room-temperature focal plane sensors [97]. Measuring voltage variations induced by THz radiation reconstructs the spatial intensity distribution. These systems directly map two-dimensional concentration profiles of pesticide residues, expanding the informational dimensionality of THz sensing platforms.

Static sensor arrays using resonance frequency matching, pixelated spatiospectral encoding platforms, and focal plane imaging systems advance multi-target detection and chemical visualization. Current limitations include array architecture complexity, the requirement for optimized multi-channel data deconvolution algorithms, and system integration demands. Integrating programmable information metamaterials, dynamic modulation mechanisms, and machine learning data processing enables intelligent platforms for simultaneous sensing and imaging. These platforms advance applications in real-time environmental monitoring, rapid food safety screening, and precision biomedical diagnostics.

Liquid biopsy presents a critical application domain for terahertz intelligent sensing. Conventional oncological diagnostics depend on invasive tissue sampling. Liquid biopsy offers a minimally invasive alternative for precision medicine by analyzing biofluids such as blood or saliva. Terahertz metamaterial sensors enable the label-free detection of disease biomarkers, including circulating tumor DNA (ctDNA), exosomes, and low-abundance proteins [98]. The inherently low concentration of these targets in complex biological matrices requires analytical platforms with high sensitivity and specificity. High-Q metasurfaces address the sensitivity requirement through strong electromagnetic field confinement. Integrating specific surface functionalization, such as aptamers targeting exosomal surface proteins, facilitates target isolation from background interference. Recent advancements in photonic sensor technologies demonstrate the necessity of pushing detection limits to achieve reliable liquid biopsy outcomes [99]. Combining terahertz sensing arrays with

microfluidic modules establishes a hardware foundation for early-stage screening and clinical diagnostics.

6. Frontiers: Intelligence, Integration, and Practical Applications

Terahertz metamaterial sensing is advancing from static devices to platforms featuring dynamic reconfigurability, multifunctional integration, and AI. This chapter examines dynamically reconfigurable metasurfaces, multimodal fusion, system-on-chip (SoC) integration, and AI data processing. The discussion analyzes scaling challenges for standardization and practical applications. These advancements enable sensing platforms with high sensitivity, specificity, rapid response times, and environmental adaptability.

Dynamically reconfigurable metasurfaces enable active control over electromagnetic responses. Integrating active tuning elements such as phase-change materials, two-dimensional materials like graphene, liquid crystals, or micro-electro-mechanical systems (MEMS) modulates resonance frequency, phase, and amplitude. Wang et al. reviewed electrical, thermal, optical, mechanical, and chemical modulation mechanisms [100]. For electrical tuning, Zhang et al. integrated varactor diodes with a graphene sandwich structure [101], achieving independent control over resonance absorption frequency (3.4 to 4.55 GHz) and amplitude (reflection coefficients from -3 to -35 dB). This dual-tuning mechanism scales to the THz and optical regimes, shown in Figure 8a. For thermal tuning, Iyer et al. utilized temperature-dependent variations in semiconductor carrier concentration and effective mass. Designing resonators on heavily doped InSb substrates [102] yielded a steady-state resonance wavelength shift exceeding 1.7 μm in the mid-infrared range. This shift surpasses the conventional thermo-optic effect, illustrated in Figure 8b.

Optical pump-probe modulation provides ultrafast control. Liu et al. used intense THz pump pulses to induce phase transitions in VO_2 metamaterials via the Poole-Frenkel effect and Joule heating [103]. This approach modulated transmissivity by 13% on a picosecond timescale, shown in Figure 8d. For mechanical tuning, Cong et al. developed a MEMS-based cantilever structure with voltage-controlled tilt angles [104]. This structure dynamically controls the output phase difference across a 360° range, enabling localized unit cell control for wavefront deflection and real-time reconfigurable holography, illustrated in Figure 8c. Real-time tunability matches a single sensor to various analyte spectra and supports multi-target detection through coded sequence switching. This establishes the hardware foundation for adaptive programmable sensing arrays.

Multimodal fusion and system-on-chip integration enhance information acquisition and practical utility [105,106]. Combining THz metamaterial sensing with analytical techniques like Raman spectroscopy [107–109] or fluorescence detection [110–112] provides comprehensive structural and compositional analysis. This fusion improves detection reliability in complex systems [113]. Miniaturization and high-level integration facilitate on-site applications [114,115]. Integrating metamaterial sensing units monolithically or heterogeneously with microfluidic modules, on-chip THz sources, and detectors creates miniaturized laboratories. This integration simplifies workflows and reduces power consumption and system volume [116–118].

Wang et al. designed a THz plasmonic sensor using a resonant gradient metasurface [119], shown in Figure 8e. Integrating this gradient metasurface with quasi-BIC resonances enables continuous broadband spectral encoding and enhanced absorption without mechanical scanning. This platform dynamically detects multiple components with a LOD of approximately 10 $\mu g \cdot mm^{-2}$. Incorporating deep neural networks (DNNs) predicts individual component concentrations in mixed analytes with 93.31% accuracy.

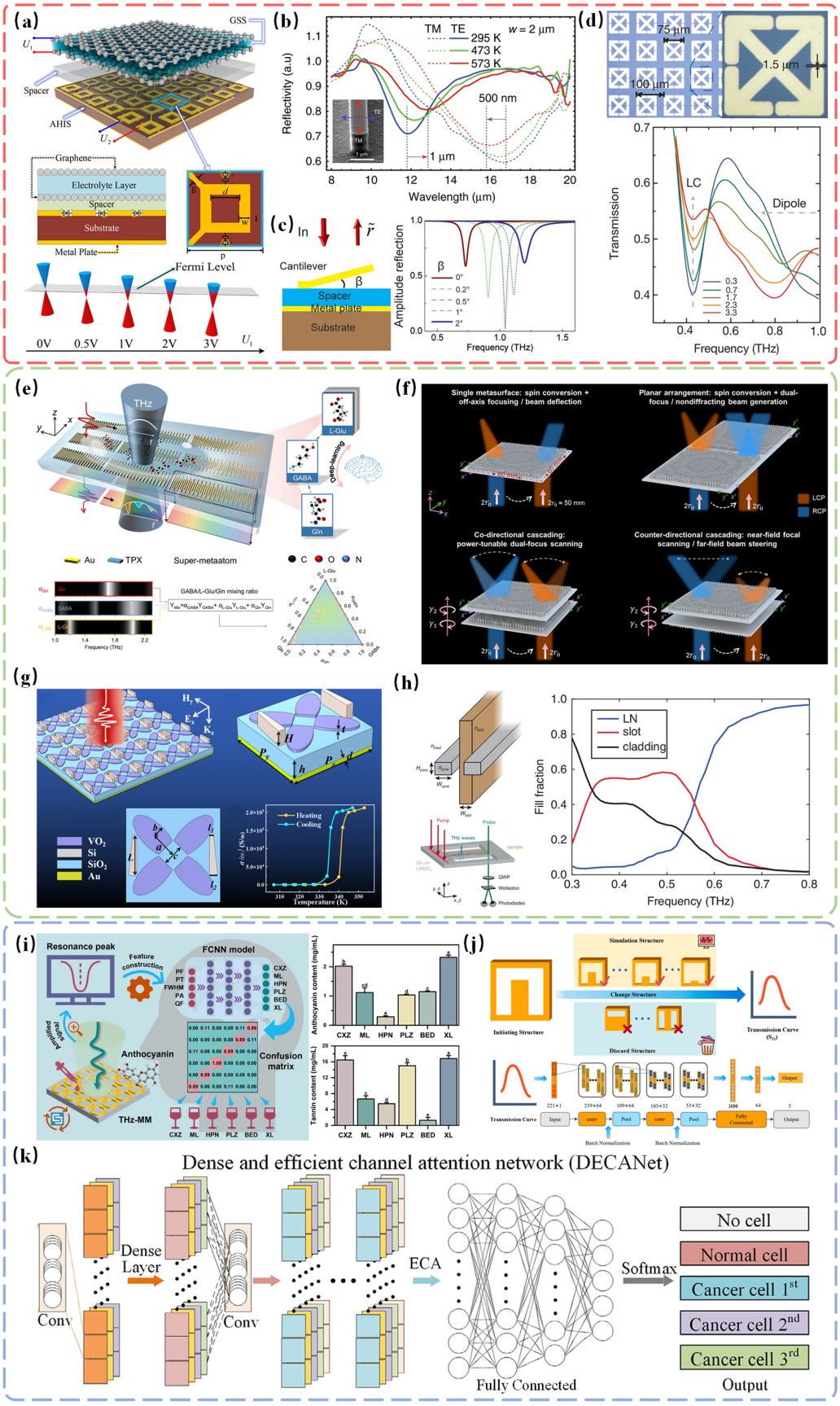

Figure 8. Frontier trends in intelligent THz sensing: dynamic reconfigurability, system-on-chip integration, and artificial intelligence empowerment. (**a**) Electrical tuning of graphene sandwich structures. Reprinted from Ref. [101] Reprinted with permission from REFERENCE CITATION. Copyright YEAR American Chemical Society. (**b**) Thermal tuning using InSb substrates. Reprinted

from Ref. [102] Copyright 2017, The Author(s), Licensed under the Creative Commons Attribution CC BY 4.0. (**c**) Mechanical tuning via MEMS-based cantilevers. Reprinted from Ref. [120] Copyright 2023, The Author(s), Licensed under the Creative Commons Attribution CC BY 4.0. (**d**) Optical pump-probe modulation of VO_2 metamaterials. Reprinted from Ref. [121] Copyright 2024, The Author(s), Licensed under the Creative Commons Attribution CC BY 4.0. (**e**) A THz plasmonic sensor based on a resonant gradient metasurface combined with deep neural networks, predicting individual component concentrations in mixed analytes with over 93% accuracy. Reprinted from Ref. [119] Copyright 2025, The Author(s), Licensed under the Creative Commons Attribution CC BY 4.0. (**f**) Spin-decoupled metasurfaces for switchable wavefront manipulation. Reprinted from Ref. [122] Reprinted with permission from REFERENCE CITATION. Copyright YEAR John Wiley and Sons. (**g**) A dual-mode tunable absorber leveraging the phase-change properties of VO_2. Reprinted from Ref. [123] 2025 Used with permission of Royal Society of Chemistry, permission conveyed through Copyright Clearance Center, Inc. (**h**) Compact THz absorption spectroscopy using $LiNbO_3$ slot waveguides, eliminating free-space optical paths to facilitate low-cost portable sensing terminals. Reprinted from Ref. [124] Copyright 2026, The Author(s), Licensed under the Creative Commons Attribution CC BY 4.0. (**i**) A deep-learning-driven dual-band sensor for red wine identification. Reprinted from Ref. [125] Copyright 2025, The Author(s), Licensed under the Creative Commons Attribution CC BY 4.0. (**j**) CNN-assisted forward optimization and inverse design of metamaterial sensors. Reprinted from Ref. [126] Copyright 2025, The Author(s), Licensed under the Creative Commons Attribution CC BY 4.0. (**k**) The DECANet deep learning framework for automated classification and high-resolution imaging of cancerous tissues, providing end-to-end diagnostic reliability for clinical applications. Reprinted from Ref. [127] Copyright 2025, The Author(s), Licensed under the Creative Commons Attribution CC BY 4.0.

Hu et al. designed a switchable multifunctional THz wave manipulation device using spin-decoupled metasurfaces [122], shown in Figure 8f. This design switches and combines multiple wavefront control functions without active materials or structural redesigns. Liu et al. proposed a dual-mode tunable THz absorber using the phase-change properties of VO_2 [123], shown in Figure 8g. The VO_2 insulator-to-metal transition (IMT) dynamically switches between narrowband and broadband absorption, reducing fabrication complexity.

Sung et al. developed a compact THz absorption spectroscopy technique using lithium niobate ($LiNbO_3$) slot waveguides [124], shown in Figure 8h. Integrating slot waveguides into thin $LiNbO_3$ layers localizes the THz electric field, enhancing measurement sensitivity for inserted samples. This method eliminates complex free-space optical paths, creating a compact system for volume-limited applications. This architecture facilitates low-cost portable sensing terminals [128,129].

To transition from bulky benchtop optical setups to fully portable system-on-chip platforms, the integration of compact terahertz illumination is required. While current metamaterial sensors exhibit excellent analytical performance, they predominantly rely on external, large-scale THz time-domain spectrometers. Future architectures must incorporate micro-sources directly onto the sensing chip. Solid-state emitters, such as terahertz quantum cascade lasers (QCLs) and resonant tunneling diodes (RTDs) [130,131], offer continuous-wave or pulsed THz radiation with sub-millimeter footprints. Implementing heterogeneous integration techniques, including flip-chip bonding and monolithic CMOS-compatible fabrication [132], enables the direct interfacing of these micro-sources with microfluidic channels and metamaterial resonators. This source-sensor integration minimizes free-space propagation losses, reduces the overall system footprint, and establishes the hardware foundation for field-deployable terahertz biochemical analysis.

AI processes complex dynamic device data [133], resolves overlapping spectra [134,135], and retrieves target information from weak signals [136,137]. For signal processing, AI models demix complex spectra, extract fingerprint features, and establish high-dimensional nonlinear mappings between spectral responses and analyte species [138–140]. For example,

Yu et al. developed a deep learning-driven dual-band THz metamaterial sensor [141], shown in Figure 8i, identifying red wine varieties with 98.33% accuracy. Chen et al. applied a convolutional neural network (CNN) assisted method [126] for forward optimization and inverse design of THz metamaterial sensors, illustrated in Figure 8j. Wang et al. developed the DECANet deep learning framework [127] for end-to-end classification of THz-TDS data, automating the identification of cancerous tissues, as shown in Figure 8k.

Despite these high reported accuracies, the integration of machine learning (ML) with THz sensing encounters primary methodological challenges related to data scarcity and model interpretability. Acquiring large-scale THz biological datasets is severely restricted by complex sample preparation and high measurement costs. Training highly parameterized deep neural networks on such limited empirical data frequently causes overfitting, compromising model generalization. To mitigate this problem, data augmentation techniques tailored for one-dimensional spectra are mandatory. Conventional approaches, including Gaussian noise addition, spectral shifting, and the synthetic minority oversampling technique (SMOTE), are used to expand the feature space. Advanced models like generative adversarial networks (GANs) can also synthesize high-fidelity THz spectral profiles to augment minority classes, significantly improving model robustness.

The opaque black-box nature of complex ML algorithms restricts their deployment in biochemical and clinical applications requiring stringent decision transparency. Reliable sensing necessitates tracing algorithmic decisions back to specific physical phenomena, such as intrinsic THz molecular resonance frequencies. Explainable AI (XAI) tools, including SHapley Additive exPlanations (SHAP) and attention mechanisms, quantify the exact contribution of specific spectral features to the final diagnostic output. Aligning these algorithmic predictions with the underlying THz physical mechanisms is essential to establish the diagnostic reliability required for clinical regulatory approval [142–144].

Transitioning these platforms from laboratory prototypes to commercial devices necessitates addressing critical manufacturability constraints, particularly fabrication tolerances and scalability. While high-Q resonances, such as quasi-BIC, provide exceptional analytical sensitivity, their performance is strictly bound by micro-nanofabrication precision. Minor geometric deviations or surface defects during large-scale manufacturing severely degrade the Q-factor and induce unpredictable spectral shifts [145]. Consequently, a fundamental physical and economic trade-off exists among achieving maximum Q-factor, ensuring operational robustness, and minimizing production costs. For practical applications, particularly in lab-on-chip biomedical sensing, selecting moderately robust resonant modes over extreme high-Q designs can mitigate batch-to-batch variability and reduce fabrication expenses. Long-term environmental stability and batch-to-batch manufacturing consistency remain critical industrialization hurdles. Addressing these issues requires durable functional materials, precise micro-nanostructure fabrication, and robust packaging technologies. Resolving these barriers demands interdisciplinary integration across materials science, micro-nanofabrication, information science, and domain-specific applications [146–149].

7. Summary and Outlook

This review summarizes the two-decade evolution of terahertz biochemical sensing from passive identification to active intelligent perception. Four technical advancements define this progression. Metamaterial field enhancement overcomes the wavelength-molecule mismatch to improve sensitivity. Surface functionalization provides molecular specificity for target confirmation. Pixelated metasurfaces transition discrete point measurements into continuous spatial mapping for multi-target visualization. Integrating dynamic reconfigurable hardware with artificial intelligence establishes system intelligence.

THz sensing provides rapid non-destructive multidimensional analysis, outperforming conventional methods. Applications include food safety screening, environmental monitoring, and biomedical diagnostics. Practical deployment faces significant hurdles. Real-world samples introduce matrix interference that degrades sensing signals. Long-term ambient device stability remains unproven. The lack of standardized performance evaluation protocols impedes cross-study comparisons and regulatory validation.

Resolving these barriers requires interdisciplinary coordination. Materials science contributes stable functional interfaces. Micro-nanofabrication provides consistent and cost-effective scalable production. Artificial intelligence must reliably process complex real-world data. Integrating these disciplines enables ubiquitous THz sensing for field-ready biochemical detection.

Beyond interdisciplinary engineering, fundamental physical advancements are necessary to overcome current platform limits. Emerging fields such as topological photonics offer an alternative physical mechanism to bypass manufacturing vulnerabilities. By exploiting topologically protected edge states, THz metasurfaces can achieve high defect immunity and environmental stability in complex real-world matrices. Additionally, exploring quantum-enhanced THz sensing represents a fundamental advancement for trace-level detection. Utilizing quantum optical phenomena, such as squeezed THz states, can push sensing limits beyond classical noise boundaries, theoretically enabling the detection of ultra-low-concentration biomarkers previously obscured by background noise.

To delineate the pathway from laboratory proof-of-concept to routine practical deployment, we propose a technology roadmap for THz intelligent sensing systems, illustrated in Figure 9. Achieving full commercialization requires surpassing specific milestones across multidisciplinary domains. In the near term, efforts must focus on establishing standardized, open-source THz spectral databases for biological and chemical analytes, coupled with robust, scalable micro-nanofabrication techniques for uniform metamaterial arrays. The mid-term milestone necessitates heterogeneous system-on-chip (SoC) integration, merging compact solid-state micro-sources (e.g., QCLs, RTDs) with sensing modules to significantly minimize system footprints. Concurrently, the deployment of XAI models must be validated to process data from complex real-world matrices, isolating target signals from background interference. Ultimately, long-term commercialization hinges on establishing rigorous regulatory evaluation protocols, conducting multi-center clinical trials for diagnostic applications, and developing advanced packaging technologies to ensure device stability in extreme environments. Overcoming these milestones will transition THz metamaterial platforms into ubiquitous, point-of-care testing (POCT) and industrial monitoring terminals.

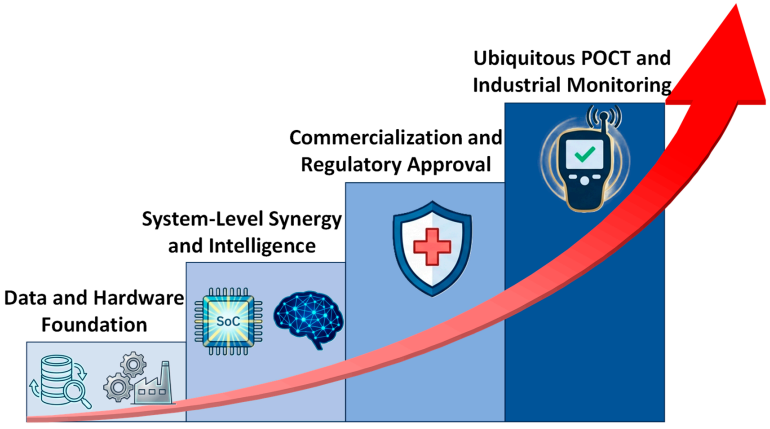

Figure 9. Technology roadmap for intelligent THz sensing systems.

Author Contributions: Conceptualization: H.Z., Y.Y.; Literature search and data curation: H.Z.; Writing—original draft preparation: H.Z.; Writing—review and editing: Z.D., Y.Y.; Visualization: H.Z.; Supervision: Z.D., Y.Y.; Project administration: Y.Y., X.R. All authors have read and agreed to the published version of the manuscript.

Funding: This work was jointly supported by the National Natural Science Foundation of China (52475462); Zhenjiang key laboratory of Advanced Manufacturing of Aerospace Components (SS2023009).

Data Availability Statement: Data sharing is not applicable.

Conflicts of Interest: The authors declare that they have no known competing financial interests or personal relationships that could have appeared to influence the work reported in this paper.

References

1. Qin, J.; Ying, Y.; Xie, L. The detection of agricultural products and food using terahertz spectroscopy: A review. *Appl. Spectrosc. Rev.* **2013**, *48*, 439–457. [CrossRef]
2. Kaltenecker, K.J.; König-Otto, J.C.; Mittendorff, M.; Winnerl, S.; Schneider, H.; Helm, M.; Helm, H.; Walther, M.; Fischer, B.M. Gouy phase shift of a tightly focused, radially polarized beam. *Optica* **2016**, *3*, 35–41. [CrossRef]
3. Islam, R.; Hasanuzzaman, G.K.M.; Habib, M.S.; Rana, S.; Khan, M.A.G. Low-loss rotated porous core hexagonal single-mode fiber in THz regime. *Opt. Fiber Technol.* **2015**, *24*, 38–43. [CrossRef]
4. Ahmadivand, A.; Gerislioglu, B.; Ramezani, Z.; Kaushik, A.; Manickam, P.; Ghoreishi, S.A. Functionalized terahertz plasmonic metasensors: Femtomolar-level detection of SARS-CoV-2 spike proteins. *Biosens. Bioelectron.* **2021**, *177*, 112971. [CrossRef]
5. Moisoiu, V.; Socaciu, A.; Stefancu, A.; Iancu, S.D.; Boros, I.; Alecsa, C.D.; Rachieriu, C.; Chiorean, A.R.; Eniu, D.; Leopold, N.; et al. Breast cancer diagnosis by surface-enhanced Raman scattering (SERS) of urine. *Appl. Sci.* **2019**, *9*, 806. [CrossRef]
6. Liu, L.; Li, T.; Liu, Z.; Fan, F.; Yuan, H.; Zhang, Z.; Chang, S.; Zhang, X. Terahertz polarization sensing based on metasurface microsensor display anti-proliferation of tumor cells with aspirin. *Biomed. Opt. Express* **2020**, *11*, 2416–2430. [CrossRef] [PubMed]
7. Ryder, M.R.; Van de Voorde, B.; Civalleri, B.; Bennett, T.D.; Mukhopadhyay, S.; Cinque, G.; Fernandez-Alonso, F.; De Vos, D.; Rudić, S.; Tan, J.C. Detecting molecular rotational dynamics complementing the low-frequency terahertz vibrations in a zirconium-based metal-organic framework. *Phys. Rev. Lett.* **2017**, *118*, 255502. [CrossRef]
8. Arora, A.; Luong, T.Q.; Krüger, M.; Kim, Y.J.; Nam, C.H.; Manz, A.; Havenith, M. Terahertz-time domain spectroscopy for the detection of PCR amplified DNA in aqueous solution. *Analyst* **2012**, *137*, 575–579. [CrossRef]
9. Petrov, V.; Moltchanov, D.; Koucheryavy, Y.; Jornet, J.M. Capacity and outage of terahertz communications with user micro-mobility and beam misalignment. *IEEE Trans. Veh. Technol.* **2020**, *69*, 6822–6827. [CrossRef]
10. Tekbıyık, K.; Ekti, A.R.; Kurt, G.K.; Görçin, A.; Yarkan, S. Modeling and analysis of short distance sub-terahertz communication channel via mixture of gamma distribution. *IEEE Trans. Veh. Technol.* **2021**, *70*, 2945–2954. [CrossRef]
11. Cheng, Y.; Wang, Y.; Niu, Y.; Zhao, Z. Concealed object enhancement using multi-polarization information for passive millimeter and terahertz wave security screening. *Opt. Express* **2020**, *28*, 6350–6366. [CrossRef]
12. Lyu, J.; Shen, S.; Chen, L.; Zhu, Y.; Zhuang, S. Frequency selective fingerprint sensor: The Terahertz unity platform for broadband chiral enantiomers multiplexed signals and narrowband molecular AIT enhancement. *PhotoniX* **2023**, *4*, 28. [CrossRef]
13. Liu, B.; Peng, Y.; Hao, Y.; Zhu, Y.; Chang, S.; Zhuang, S. Ultra-wideband terahertz fingerprint enhancement sensing and inversion model supported by single-pixel reconfigurable graphene metasurface. *PhotoniX* **2024**, *5*, 10. [CrossRef]
14. Li, Y.; Chang, C.; Zhu, Z.; Sun, L.; Fan, C. Terahertz wave enhances permeability of the voltage-gated calcium channel. *J. Am. Chem. Soc.* **2021**, *143*, 4311–4318. [CrossRef]
15. Cherkasova, E.I.; Babak, K.V.; Belotelov, A.O.; Labutina, Y.L.; Yusupov, V.I.; Vorobieva, N.N.; Nerush, A.S.; Maslennikova, A.V. A response of HeLa Kyoto tumor cells on a combination of photobiomodulation and ionizing radiation. In *Mechanisms and Techniques in Photodynamic Therapy and Photobiomodulation*; SPIE: Bellingham, WA, USA, 2021; Volume 11628.
16. Ahmadivand, A.; Gerislioglu, B.; Ahuja, R.; Mishra, Y.K. Terahertz plasmonics: The rise of toroidal metadevices towards immunobiosensings. *Mater. Today* **2020**, *32*, 108–130. [CrossRef]
17. Trainiti, G.; Xia, Y.; Marconi, J.; Cazzulani, G.; Erturk, A.; Ruzzene, M. Time-periodic stiffness modulation in elastic metamaterials for selective wave filtering: Theory and experimental investigations. *arXiv* **2018**, arXiv:1804.09209. [CrossRef]
18. Sun, X.Y.; Zheng, L.R.; Li, X.N.; Xu, H.; Liang, X.T.; Zhang, X.P.; Lu, Y.-H.; Lee, Y.-P.; Rhee, J.-Y.; Song, W.J. Origin of strain-induced resonances in flexible terahertz metamaterials. *Chin. Phys. B* **2016**, *5*, 388–392. (In Chinese) [CrossRef]
19. Han, Z.; Zhang, Y.; Bozhevolnyi, S.I. Spoof surface plasmon-based stripe antennas with extreme field enhancement in the terahertz regime. *Opt. Lett.* **2015**, *40*, 2533–2536. [CrossRef] [PubMed]

20. Pendry, J.B.; Martin-Moreno, L.; Garcia-Vidal, F.J. Mimicking surface plasmons with structured surfaces. *Science* **2004**, *305*, 847–848. [CrossRef]
21. Liu, G.-D.; Zhai, X.; Wang, L.L.; Lin, Q.; Xia, S.X.; Luo, X.; Zhao, C.J. A high-performance refractive index sensor based on Fano resonance in Si split-ring metasurface. *Plasmonics* **2018**, *13*, 15–19. [CrossRef]
22. Rahman, B.A.; Viphavakit, C.; Chitaree, R.; Ghosh, S.; Pathak, A.K.; Verma, S.; Sakda, N. Optical fiber, nanomaterial, and thz-metasurface-mediated nano-biosensors: A Review. *Biosensors* **2022**, *12*, 42. [CrossRef]
23. Zhang, Z.; Zhao, R.; Cong, M.; Qiu, J. Developments of terahertz metasurface biosensors: A literature review. *Nanotechnol. Rev.* **2024**, *13*, 20230182. [CrossRef]
24. Yang, K.; Li, J.; De La Chapelle, M.L.; Huang, G.; Wang, Y.; Zhang, J.; Xu, D.; Yao, J.; Yang, X.; Fu, W. A terahertz metamaterial biosensor for sensitive detection of microRNAs based on gold-nanoparticles and strand displacement amplification. *Biosens. Bioelectron.* **2021**, *175*, 112874. [CrossRef] [PubMed]
25. Zhao, X.; Lin, Z.; Wang, Y.; Yang, X.; Yang, K.; Zhang, Y.; Peng, J.; de la Chapelle, M.L.; Zhang, L.; Fu, W. Label-free self-referenced sensing of living cells by terahertz metamaterial-based reflection spectroscopy. *Biomed. Opt. Express* **2019**, *10*, 1196–1206. [CrossRef]
26. Geng, Z.; Zhang, X.; Fan, Z.; Lv, X.Q.; Chen, H.D. A route to terahertz metamaterial biosensor integrated with microfluidics for liver cancer biomarker testing in early stage. *Sci. Rep.* **2017**, *7*, 16378. [CrossRef]
27. Lee, S.-H.; Choe, J.H.; Kim, C.; Bae, S.; Kim, J.S.; Park, Q.H.; Seo, M. Graphene assisted terahertz metamaterials for sensitive bio-sensing. *Sens. Actuators B Chem.* **2020**, *310*, 127841. [CrossRef]
28. Yu, N.; Aieta, F.; Genevet, P.; Kats, M.A.; Gaburro, Z.; Capasso, F. A broadband, background-free quarter-wave plate based on plasmonic metasurfaces. *Nano Lett.* **2012**, *12*, 6328–6333. [CrossRef]
29. Lee, G.-Y.; Yoon, G.; Lee, S.Y.; Yun, H.; Cho, J.; Lee, K.; Kim, H.; Rho, J.; Lee, B. Complete amplitude and phase control of light using broadband holographic metasurfaces. *Nanoscale* **2018**, *10*, 4237–4245. [CrossRef]
30. Zhang, K.; Yuan, Y.; Zhang, D.; Ding, X.; Ratni, B.; Burokur, S.N.; Lu, M.; Tang, K.; Wu, Q. Phase-engineered metalenses to generate converging and non-diffractive vortex beam carrying orbital angular momentum in microwave region. *Opt. Express* **2018**, *26*, 1351–1360. [CrossRef]
31. Maguid, E.; Yulevich, I.; Yannai, M.; Kleiner, V.; Brongersma, M.L.; Hasman, E. Multifunctional interleaved geometric-phase dielectric metasurfaces. *Light Sci. Appl.* **2017**, *6*, e17027. [CrossRef] [PubMed]
32. Almeida, E.; Shalem, G.; Prior, Y. Subwavelength nonlinear phase control and anomalous phase matching in plasmonic metasurfaces. *Nat. Commun.* **2016**, *7*, 10367. [CrossRef]
33. Shelby, R.A.; Smith, D.R.; Schultz, S. Experimental verification of a negative index of refraction. *Science* **2001**, *292*, 77–79. [CrossRef]
34. Chu, H.; Li, Q.; Liu, B.; Luo, J.; Sun, S.; Hang, Z.H.; Zhou, L.; Lai, Y. A hybrid invisibility cloak based on integration of transparent metasurfaces and zero-index materials. *Light Sci. Appl.* **2018**, *7*, 50. [CrossRef]
35. Liu, Y.J.; Hao, Q.; Smalley, J.S.; Liou, J.; Khoo, I.C.; Huang, T.J. A frequency-addressed plasmonic switch based on dual-frequency liquid crystals. *Appl. Phys. Lett.* **2010**, *97*, 091101. [CrossRef]
36. Bomzon, Z.; Biener, G.; Kleiner, V.; Hasman, E. Space-variant Pancharatnam–Berry phase optical elements with computer-generated subwavelength gratings. *Opt. Lett.* **2002**, *27*, 1141–1143. [CrossRef]
37. Sun, S.; He, Q.; Xiao, S.; Xu, Q.; Li, X.; Zhou, L. Gradient-index meta-surfaces as a bridge linking propagating waves and surface waves. *Nat. Mater.* **2012**, *11*, 426–431. [CrossRef] [PubMed]
38. Sun, S.; Yang, K.Y.; Wang, C.M.; Juan, T.K.; Chen, W.T.; Liao, C.Y.; He, Q.; Xiao, S.; Kung, W.-T.; Guo, G.-Y.; et al. High-efficiency broadband anomalous reflection by gradient meta-surfaces. *Nano Lett.* **2012**, *12*, 6223–6229. [CrossRef] [PubMed]
39. Xie, X.; Pu, M.; Liu, K.; Ma, X.; Li, X.; Yang, J.; Luo, X. High-Efficiency and Tunable Circular-Polarization Beam Splitting with a Liquid-Filled All-Metallic Catenary Meta-Mirror. *Adv. Mater. Technol.* **2019**, *4*, 1900334. [CrossRef]
40. Hu, M.; Chen, J.; Li, Z.Y.; Au, L.; Hartland, G.V.; Li, X.; Marquez, M.; Xia, Y. Gold nanostructures: Engineering their plasmonic properties for biomedical applications. *Chem. Soc. Rev.* **2006**, *35*, 1084–1094. [CrossRef]
41. Liu, Y.J.; Si, G.Y.; Leong, E.S.; Xiang, N.; Danner, A.J.; Teng, J.H. Light-driven plasmonic color filters by overlaying photoresponsive liquid crystals on gold annular aperture arrays. *Adv. Mater.* **2012**, *24*, OP131–OP135. [CrossRef]
42. Chen, Y.G.; Kao, T.S.; Ng, B.; Li, X.; Luo, X.G.; Luk'Yanchuk, B.; Maier, S.A.; Hong, M.H. Hybrid phase-change plasmonic crystals for active tuning of lattice resonances. *Opt. Express* **2013**, *21*, 13691–13698. [CrossRef] [PubMed]
43. Yu, N.; Genevet, P.; Kats, M.A.; Aieta, F.; Tetienne, J.P.; Capasso, F.; Gaburro, Z. Light propagation with phase discontinuities: Generalized laws of reflection and refraction. *Science* **2011**, *334*, 333–337. [CrossRef] [PubMed]
44. Capasso, F. The future and promise of flat optics: A personal perspective. *Nanophotonics* **2018**, *7*, 953–957. [CrossRef]
45. Kamali, S.M.; Arbabi, E.; Arbabi, A.; Faraon, A. A review of dielectric optical metasurfaces for wavefront control. *Nanophotonics* **2018**, *7*, 1041–1068. [CrossRef]
46. West, P.R.; Stewart, J.L.; Kildishev, A.V.; Shalaev, V.M.; Shkunov, V.V.; Strohkendl, F.; Zakharenkov, Y.A.; Dodds, R.K.; Byren, R. All-dielectric subwavelength metasurface focusing lens. *Opt. Express* **2014**, *22*, 26212–26221. [CrossRef]

47. Yang, X.; Zhao, X.; Yang, K.; Liu, Y.; Liu, Y.; Fu, W.; Luo, Y. Biomedical applications of terahertz spectroscopy and imaging. *Trends Biotechnol.* **2016**, *34*, 810–824. [CrossRef]
48. Nie, P.; Zhu, D.; Cui, Z.; Qu, F.; Lin, L.; Wang, Y. Sensitive detection of chlorpyrifos pesticide using an all-dielectric broadband terahertz metamaterial absorber. *Sens. Actuators B Chem.* **2020**, *307*, 127642. [CrossRef]
49. Wang, Q.; Yin, S.; Shi, X.; Fan, J.; Huang, K.; Gao, W.; Xie, L.; Ying, Y. High-sensitivity detection of trace imidacloprid and tetracycline hydrochloride by multi-frequency resonance metamaterials. *J. Food Meas. Charact.* **2022**, *16*, 2041–2048. [CrossRef]
50. Li, J.; Sun, K.; He, W.; Chen, K.; Ge, L.; Zhong, K.; Wang, Y.; Xu, D.; Yao, J. THz plasmon-induced transparency metasurfaces based on metal-graphene hybrid structure for high-sensitive amino acid disease-marker biosensing. *Results Phys.* **2023**, *44*, 106184. [CrossRef]
51. Zhang, Y.; Xu, Y.; Liu, H.; Sun, B. Ultrahigh sensitivity nitrogen-doping carbon nanotubes-based metamaterial-free flexible terahertz sensing platform for insecticides detection. *Food Chem.* **2022**, *394*, 133467. [CrossRef]
52. Du, X.; Mao, H.; Yan, Y.; Zhang, X.; Wang, Y.; Liu, Y.; Wang, B.; Yang, X.; Shi, Q. Study on the spectral characteristics of plant growth regulators based on the structure difference of terahertz metamaterial sensor. *IEEE Sens. J.* **2022**, *22*, 14065–14074. [CrossRef]
53. Dai, Z.; Su, Q.; Lu, D.; Sun, L.; Liu, W. A combined experimental and theoretical study on the terahertz vibrations of water vapors. *Spectrochim. Acta Part A Mol. Biomol. Spectrosc.* **2019**, *214*, 277–284. [CrossRef]
54. Zhou, R.; Wang, C.; Huang, Y.; Huang, K.; Wang, Y.; Xu, W.; Xie, L.; Ying, Y. Label-free terahertz microfluidic biosensor for sensitive DNA detection using graphene-metasurface hybrid structures. *Biosens. Bioelectron.* **2021**, *188*, 113336. [CrossRef] [PubMed]
55. Lee, S.-H.; Lee, D.; Choi, M.H.; Son, J.H.; Seo, M. Highly sensitive and selective detection of steroid hormones using terahertz molecule-specific sensors. *Anal. Chem.* **2019**, *91*, 6844–6849. [CrossRef]
56. Zhou, J.; Zhao, X.; Huang, G.; Yang, X.; Zhang, Y.; Zhan, X.; Tian, H.; Xiong, Y.; Wang, Y.; Fu, W. Molecule-specific terahertz biosensors based on an aptamer hydrogel-functionalized metamaterial for sensitive assays in aqueous environments. *ACS Sens.* **2021**, *6*, 1884–1890. [CrossRef] [PubMed]
57. Xu, W.; Xie, L.; Zhu, J.; Xu, X.; Ye, Z.; Wang, C.; Ma, Y.; Ying, Y. Gold nanoparticle-based terahertz metamaterial sensors: Mechanisms and applications. *ACS Photonics* **2016**, *3*, 2308–2314. [CrossRef]
58. Seo, M.; Park, H.-R. Terahertz biochemical molecule-specific sensors. *Adv. Opt. Mater.* **2020**, *8*, 1900662. [CrossRef]
59. Burford, N.M.; El-Shenawee, M.O. Review of terahertz photoconductive antenna technology. *Opt. Eng.* **2017**, *56*, 010901. [CrossRef]
60. Viti, L.; Riccardi, E.; Beere, H.E.; Ritchie, D.A.; Vitiello, M.S. Real-time measure of the lattice temperature of a semiconductor heterostructure laser via an on-chip integrated graphene thermometer. *ACS Nano* **2023**, *17*, 6103–6112. [CrossRef]
61. Wang, P.; Lou, J.; Yu, Y.; Sun, L.; Sun, L.; Fang, G.; Chang, C. An ultra-sensitive metasurface biosensor for instant cancer detection based on terahertz spectra. *Nano Res.* **2023**, *16*, 7304–7311. [CrossRef]
62. Zhang, C.; Xue, T.; Zhang, J.; Liu, L.; Xie, J.; Wang, G.; Yao, J.; Zhu, W.; Ye, X. Terahertz toroidal metasurface biosensor for sensitive distinction of lung cancer cells. *Nanophotonics* **2021**, *11*, 101–109. [CrossRef]
63. Saadatmand, S.B.; Ahmadi, V.; Hamidi, S.M. Quasi-BIC based all-dielectric metasurfaces for ultra-sensitive refractive index and temperature sensing. *Sci. Rep.* **2023**, *13*, 20625. [CrossRef]
64. Wang, Q.; Chen, Y.; Mao, J.; Yang, F.; Wang, N. Metasurface-assisted terahertz sensing. *Sensors* **2023**, *23*, 5902. [CrossRef]
65. Wei, X.; Ren, C.; Liu, B.; Peng, Y.; Zhuang, S. The theory, technology, and application of terahertz metamaterial biosensors: A review. *Fundam. Res.* **2025**, *5*, 571–585. [CrossRef] [PubMed]
66. Ye, Y.; Zhang, Y.; Zhao, Y.; Ren, Y.; Ren, X. Sensitivity influencing factors during pesticide residue detection research via a terahertz metasensor. *Opt. Express* **2021**, *29*, 15255–15268. [CrossRef] [PubMed]
67. Chao, R.; Xu, X.; Li, Y.; Kuang, X.; Liu, J.; Du, Y. Sensitive detection of glucose enantiomers using open-ring resonator-based metamaterial sensor. *J. Appl. Phys.* **2025**, *138*, 163102. [CrossRef]
68. Hsu, C.W.; Zhen, B.; Lee, J.; Chua, S.L.; Johnson, S.G.; Joannopoulos, J.D.; Soljačić, M. Observation of trapped light within the radiation continuum. *Nature* **2013**, *499*, 188–191. [CrossRef]
69. Cong, L.; Singh, R. Symmetry-protected dual bound states in the continuum in metamaterials. *Adv. Opt. Mater.* **2019**, *7*, 1900383. [CrossRef]
70. Zhang, Z.; Yang, L.; Fan, J.; Chen, X.; Chen, X.; Zhou, H.; Ma, Y.; Li, R. Terahertz angle sensor based on the asymmetry coupling of the square and L-shaped structure. *Photonics Nanostructures-Fundam. Appl.* **2024**, *61*, 101288. [CrossRef]
71. Peng, J.; Lin, X.; Yan, X.; Yan, X.; Hu, X.; Yao, H.; Liang, L.; Ma, G. Terahertz biosensor engineering based on quasi-BIC metasurface with ultrasensitive detection. *Nanomaterials* **2024**, *14*, 799. [CrossRef]
72. Wang, Y.; Han, Z.; Du, Y.; Qin, J. Ultrasensitive terahertz sensing with high-Q toroidal dipole resonance governed by bound states in the continuum in all-dielectric metasurface. *Nanophotonics* **2021**, *10*, 1295–1307. [CrossRef]

73. Liu, B.; Peng, Y.; Jin, Z.; Wu, X.; Gu, H.; Wei, D.; Zhu, Y.; Zhuang, S. Terahertz ultrasensitive biosensor based on wide-area and intense light-matter interaction supported by QBIC. *Chem. Eng. J.* **2023**, *462*, 10–1016. [CrossRef]
74. Tang, J.; Ye, Y.; Xu, J.; Zheng, Z.; Jin, X.; Jiang, L.; Jiang, J.; Xiang, Y. High-sensitivity terahertz refractive index sensor in a multilayered structure with graphene. *Nanomaterials* **2020**, *10*, 500. [CrossRef]
75. Zhao, R.; Ye, Y.; Dai, Z.; Mu, T.; Ren, X. Research on specific identification method of substances through terahertz metamaterial sensors. *Results Phys.* **2022**, *43*, 106055. [CrossRef]
76. Li, X.; Jiao, H.; Zhu, M.; Deng, T.; Sun, J. A novel terahertz integrated sensor for liquid samples detections based on metamaterial and embedded microfluidic channels. *J. Phys. D Appl. Phys.* **2023**, *56*, 025401. [CrossRef]
77. Xu, X.; Zheng, D.; Lin, Y.-S. Electric split-ring metamaterial based microfluidic chip with multi-resonances for microparticle trapping and chemical sensing applications. *J. Colloid Interface Sci.* **2023**, *642*, 462–469. [CrossRef]
78. Ahmadivand, A.; Gerislioglu, B.; Manickam, P.; Kaushik, A.; Bhansali, S.; Nair, M.; Pala, N. Rapid detection of infectious envelope proteins by magnetoplasmonic toroidal metasensors. *ACS Sens.* **2017**, *2*, 1359–1368. [CrossRef]
79. Lyu, J.; Huang, L.; Chen, L.; Zhu, Y.; Zhuang, S. Review on the terahertz metasensor: From featureless refractive index sensing to molecular identification. *Photonics Res.* **2024**, *12*, 194–217. [CrossRef]
80. Liu, W.; Hu, F.; Lin, S.; Zeng, L.; Jiang, M.; Zhang, L.; Zou, Y. High sensitive and specific detection of SCCA via halloysite nanotube modified terahertz metasurface sensor. *IEEE Sens. J.* **2023**, *23*, 6728–6733. [CrossRef]
81. Zhang, M.; Zhang, S.; Wang, Q.; Xu, Y.; Jiang, L.; Yan, Y.; Li, J.; Tian, Z.; Zhang, W. Flexible Specific Determination of Glucose in Solution, Blood Serum, and Sweat Using a Terahertz Hydrogel-Functionalized Metamaterial. *Adv. Mater. Technol.* **2023**, *8*, 2300775. [CrossRef]
82. Xu, W.; Xie, L.; Zhu, J.; Tang, L.; Singh, R.; Wang, C.; Ma, Y.; Chen, H.-T.; Ying, Y. Terahertz biosensing with a graphene-metamaterial heterostructure platform. *Carbon* **2019**, *141*, 247–252. [CrossRef]
83. Shi, W.; Fan, F.; Li, S.; Zhang, Z.; Liu, H.; Wang, X.; Chang, S. Terahertz immunosensing assisted by functionalized Au NPs based on all-dielectric metasurface. *Sens. Actuators B Chem.* **2022**, *362*, 131777. [CrossRef]
84. Niu, Q.; Fu, L.; Zhong, Y.; Cui, B.; Zhang, G.; Yang, Y. Sensitive and specific detection of carcinoembryonic antigens using toroidal metamaterial biosensors integrated with functionalized gold nanoparticles. *Anal. Chem.* **2022**, *95*, 1123–1131. [CrossRef]
85. Beruete, M.; Jáuregui-López, I. Terahertz sensing based on metasurfaces. *Adv. Opt. Mater.* **2020**, *8*, 1900721. [CrossRef]
86. Weis, P.; Garcia-Pomar, J.L.; Beigang, R.; Rahm, M. Hybridization induced transparency in composites of metamaterials and atomic media. *Opt. Express* **2011**, *19*, 23573–23580. [CrossRef] [PubMed]
87. Chen, X.; Xin, S.; Liu, Q.; Meng, Y.; Yu, D.; Tseng, M.L.; Ye, L. Dielectric metasurface-assisted terahertz sensing: Mechanism, fabrication, and multiscenario applications. *Nanophotonics* **2025**, *14*, 271–296. [CrossRef] [PubMed]
88. Zhong, Y.; Du, L.; Liu, Q.; Zhu, L.; Meng, K.; Zou, Y.; Zhang, B. Ultrasensitive specific sensor based on all-dielectric metasurfaces in the terahertz range. *RSC Adv.* **2020**, *10*, 33018–33025. [CrossRef] [PubMed]
89. Kawase, K.; Ogawa, Y.; Watanabe, Y.; Inoue, H. Non-destructive terahertz imaging of illicit drugs using spectral fingerprints. *Opt. Express* **2003**, *11*, 2549–2554. [CrossRef]
90. Ye, Y.; Zhang, H.; Yang, S.; Dai, Z.; Ren, X. Terahertz metamaterial sensor for specific detection of pesticides based on spectroscopy and imaging. *Acta Opt. Sin.* **2026**, *46*, 03.
91. Sun, L.; Xu, L.; Wang, J.; Jiao, Y.; Ma, Z.; Ma, Z.; Chang, C.; Yang, X.; Wang, R. A pixelated frequency-agile metasurface for broadband terahertz molecular fingerprint sensing. *Nanoscale* **2022**, *14*, 9681–9685. [CrossRef]
92. Jin, Z.; Lou, J.; Shu, F.; Hong, Z.; Qiu, C.W. Advances in nanoengineered terahertz technology: Generation, modulation, and bio-applications. *Research* **2025**, *8*, 0562. [CrossRef]
93. Fu, X.; Shi, L.; Cui, T. Research progress in terahertz metamaterials and their applications in imaging. *J. Mater. Eng.* **2020**, *48*, 12–22.
94. Tittl, A.; Leitis, A.; Liu, M.; Yesilkoy, F.; Choi, D.Y.; Neshev, D.N.; Kivshar, Y.S.; Altug, H. Imaging-based molecular barcoding with pixelated dielectric metasurfaces. *Science* **2018**, *360*, 1105–1109. [CrossRef]
95. Watts, C.M.; Shrekenhamer, D.; Montoya, J.; Lipworth, G.; Hunt, J.; Sleasman, T.; Krishna, S.; Smith, D.R.; Padilla, W.J. Terahertz compressive imaging with metamaterial spatial light modulators. *Nat. Photonics* **2014**, *8*, 605–609. [CrossRef]
96. Kuznetsov, S.A.; Paulish, A.G.; Gelfand, A.V.; Lazorskiy, P.A.; Fedorinin, V.N. Matrix structure of metamaterial absorbers for multispectral terahertz imaging. *Prog. Electromagn. Res.* **2012**, *122*, 93–103. [CrossRef]
97. Escorcia, I.; Grant, J.; Gough, J.; Cumming, D.R. Uncooled CMOS terahertz imager using a metamaterial absorber and pn diode. *Opt. Lett.* **2016**, *41*, 3261–3264. [CrossRef] [PubMed]
98. Jia, Q.; Ma, Z.; Wang, Y.; Zhang, M.; Zou, G.; Lan, B.; Li, S.; Lao, Z.; Shen, W.; Lou, J.; et al. Integrated single-step terahertz metasensing for simultaneous detection based on exosomal membrane proteins enables pathological typing of gastric cancer. *Research* **2025**, *8*, 0625. [CrossRef] [PubMed]
99. Colapietro, P.; Brunetti, G.; Panciera, C.; Elicio, A.; Ciminelli, C. Shining the path of precision diagnostic: Advancements in photonic sensors for liquid biopsy. *Biosensors* **2025**, *15*, 473. [CrossRef]

100. Wang, J.; Li, K.; Cheng, M.; Chen, L.; Kong, D.; Liu, Y. Research progress and applications of dynamically tunable metasurfaces. *Opto-Electron. Eng.* **2025**, *50*, 230141.
101. Zhang, J.; Wei, X.; Rukhlenko, I.D.; Chen, H.T.; Zhu, W. Electrically tunable metasurface with independent frequency and amplitude modulations. *Acs Photonics* **2019**, *7*, 265–271. [CrossRef]
102. Iyer, P.P.; Pendharkar, M.; Palmstrøm, C.J.; Schuller, J.A. Ultrawide thermal free-carrier tuning of dielectric antennas coupled to epsilon-near-zero substrates. *Nat. Commun.* **2017**, *8*, 472. [CrossRef]
103. Liu, M.; Hwang, H.Y.; Tao, H.; Strikwerda, A.C.; Fan, K.; Keiser, G.R.; Sternbach, A.J.; West, K.G.; Kittiwatanakul, S.; Lu, J.; et al. Terahertz-field-induced insulator-to-metal transition in vanadium dioxide metamaterial. *Nature* **2012**, *487*, 345–348. [CrossRef]
104. Cong, L.; Pitchappa, P.; Wu, Y.; Ke, L.; Lee, C.; Singh, N.; Yang, H.; Singh, R. Active multifunctional microelectromechanical system metadevices: Applications in polarization control, wavefront deflection, and holograms. *Adv. Opt. Mater.* **2017**, *5*, 1600716.
105. Fakhlaei, R.; Babadi, A.A.; Sun, C.; Ariffin, N.M.; Khatib, A.; Selamat, J.; Xiaobo, Z. Application, challenges and future prospects of recent nondestructive techniques based on the electromagnetic spectrum in food quality and safety. *Food Chem.* **2024**, *441*, 138402. [CrossRef] [PubMed]
106. Ma, L.; Yang, X.; Xue, S.; Zhou, R.; Wang, C.; Guo, Z.; Wang, Y.; Cai, J. "Raman plus X" dual-modal spectroscopy technology for food analysis: A review. *Compr. Rev. Food Sci. Food Saf.* **2025**, *24*, e70102. [CrossRef]
107. Li, H.; Hu, W.; Hassan, M.M.; Zhang, Z.; Chen, Q. A facile and sensitive SERS-based biosensor for colormetric detection of acetamiprid in green tea based on unmodified gold nanoparticles. *J. Food Meas. Charact.* **2019**, *13*, 259–268. [CrossRef]
108. Hassan, M.M.; Xu, Y.; Zareef, M.; Li, H.; Rong, Y.; Chen, Q. Recent advances of nanomaterial-based optical sensor for the detection of benzimidazole fungicides in food: A review. *Crit. Rev. Food Sci. Nutr.* **2023**, *63*, 2851–2872. [CrossRef]
109. Sun, Y.; Zhai, X.; Xu, Y.; Liu, C.; Zou, X.; Li, Z.; Shi, J.; Huang, X. Facile fabrication of three-dimensional gold nanodendrites decorated by silver nanoparticles as hybrid SERS-active substrate for the detection of food contaminants. *Food Control* **2021**, *122*, 107772.
110. Wang, P.; Li, H.; Hassan, M.M.; Guo, Z.; Zhang, Z.Z.; Chen, Q. Fabricating an acetylcholinesterase modulated UCNPs-Cu2+ fluorescence biosensor for ultrasensitive detection of organophosphorus pesticides-diazinon in food. *J. Agric. Food Chem.* **2019**, *67*, 4071–4079. [PubMed]
111. Xu, Y.; Hassan, M.M.; Sharma, A.S.; Li, H.; Chen, Q. Recent advancement in nano-optical strategies for detection of pathogenic bacteria and their metabolites in food safety. *Crit. Rev. Food Sci. Nutr.* **2023**, *63*, 486–504. [CrossRef]
112. Wang, L.; Haruna, S.A.; Ahmad, W.; Wu, J.; Chen, Q.; Ouyang, Q. Tunable multiplexed fluorescence biosensing platform for simultaneous and selective detection of paraquat and carbendazim pesticides. *Food Chem.* **2022**, *388*, 132950. [CrossRef]
113. Dong, X.; Huang, A.; He, L.; Cai, C.; You, T. Recent advances in foodborne pathogen detection using photoelectrochemical biosensors: From photoactive material to sensing strategy. *Front. Sustain. Food Syst.* **2024**, *8*, 1432555. [CrossRef]
114. Tong, Y.; Wang, S.; Han, K.; Song, X.; Zhang, W.; Ye, Y.; Ren, X. Development of a novel metal grating and its applications of terahertz spectroscopic detection of CuSO4 in fruit. *Food Anal. Methods* **2021**, *14*, 1590–1599. [CrossRef]
115. Tong, Y.; Ding, L.; Han, K.; Zou, X.; Wang, S.; Wen, Z.; Ye, Y.; Ren, X. Detection of carbendazim in oranges with metal grating integrated microfluidic sensor in terahertz. *Food Addit. Contam. Part A* **2022**, *39*, 1555–1564. [CrossRef] [PubMed]
116. Zhang, X.; Duan, Z.; Mao, H.; Gao, H.; Zuo, Z. A lettuce moisture detection method based on terahertz time-domain spectroscopy. *Ciência Rural* **2021**, *52*, e20210002. [CrossRef]
117. Zhang, X.; Wang, P.; Mao, H.; Gao, H.; Li, Q. Detection of the nutritional status of phosphorus in lettuce using THz time-domain spectroscopy. *Eng. Agrícola* **2021**, *41*, 599–608. [CrossRef]
118. Yang, J.; Bai, X.; Wei, M.; Jiang, H.; Xu, L. Terahertz spectroscopy for food quality assessment: A comprehensive review. *Foods* **2025**, *14*, 2199. [CrossRef]
119. Wang, R.; Zhang, D.; Chen, L.; Zhang, N.; Li, D.; Jiang, R.; Zhang, X.; Yang, X.; Zhang, L.; Wang, S.; et al. Ultra-compact broadband terahertz spectroscopy sensor enabled by resonant-gradient metasurface. *Nat. Commun.* **2025**, *16*, 11462. [CrossRef] [PubMed]
120. Zhang, Z.; Shi, H.; Wang, L.; Chen, J.; Chen, X.; Yi, J.; Zhang, A.; Liu, H. Recent advances in reconfigurable metasurfaces: Principle and applications. *Nanomaterials* **2023**, *13*, 534. [CrossRef]
121. Li, C.; Pan, R.; Gu, C.; Guo, H.; Li, J. Reconfigurable micro/nano-optical devices based on phase transitions: From materials, mechanisms to applications. *Adv. Sci.* **2024**, *11*, 2306344. [CrossRef]
122. Hu, H.; Sun, Z.; Hu, X.; Wang, X. Modular Spin-Decoupled Metasurfaces for Switchable and Multifunctional Terahertz Wave Modulation. *Laser Photonics Rev.* **2025**, e02604. [CrossRef]
123. Liu, T.; Wang, C.; Zou, G.; Ji, J.; Yi, Z. A multifunctional terahertz device based on vanadium dioxide metamaterials that switches between ultra-broadband absorption and ultra-high-Q narrowband absorption. *Nanoscale Horiz.* **2025**, *10*, 3105–3115. [CrossRef]
124. Sung, E.R.; Nelson, K.A. Compact THz absorption spectroscopy using a LiNbO3 slot waveguide. *Light Sci. Appl.* **2026**, *15*, 47. [CrossRef]
125. Yu, P.; Shen, C.; Zhu, W.; Zhang, W.; Cheng, J.; Song, J. Recent Developments and Applications of Terahertz Spectroscopy in Food Analysis. *Biosensors* **2025**, *15*, 677. [CrossRef]

126. Chen, S.; Zhao, C.; Wang, W.; Yang, S.; Zhou, C. Convolutional neural network-assisted design and validation of terahertz metamaterial sensor. *Mater. Des.* **2025**, *253*, 113871. [CrossRef]
127. Wang, X.; Xu, Y.; Wang, R.; Tian, N.; Zhu, Z.; Fan, S.; Zhang, L.; Yan, R.; Chen, X. Deep learning-assisted terahertz intelligent detection and identification of cancer tissue. *Fundam. Res.* **2025**, *5*, 1831–1842. [CrossRef] [PubMed]
128. Zhang, X.; Huang, C.; Jiang, Y.; Jiang, Y.; Shen, J.; Han, E. Structure-switching electrochemical aptasensor for single-step and specific detection of trace mercury in dairy products. *J. Agric. Food Chem.* **2018**, *66*, 10106–10112. [CrossRef]
129. Jiang, L.; Wei, D.; Zeng, K.; Shao, J.; Zhu, F.; Du, D. An enhanced direct competitive immunoassay for the detection of kanamycin and tobramycin in milk using multienzyme-particle amplification. *Food Anal. Methods* **2018**, *11*, 2066–2075. [CrossRef]
130. Khalatpour, A.; Paulsen, A.K.; Deimert, C.; Wasilewski, Z.R.; Hu, Q. High-power portable terahertz laser systems. *Nat. Photonics* **2021**, *15*, 16–20. [CrossRef]
131. Cimbri, D.; Wang, J.; Al-Khalidi, A.; Wasige, E. Resonant tunneling diodes high-speed terahertz wireless communications-a review. *IEEE Trans. Terahertz Sci. Technol.* **2022**, *12*, 226–244. [CrossRef]
132. Sengupta, K.; Nagatsuma, T.; Mittleman, D.M. Terahertz integrated electronic and hybrid electronic–photonic systems. *Nat. Electron.* **2018**, *1*, 622–635. [CrossRef]
133. Lun, Z.; Wu, X.; Dong, J.; Wu, B. Deep learning-enhanced spectroscopic technologies for food quality assessment: Convergence and emerging frontiers. *Foods* **2025**, *14*, 2350. [CrossRef]
134. Adade, S.Y.-S.S.; Lin, H.; Nunekpeku, X.; Johnson, N.A.N.; Agyekum, A.A.; Zhao, S.; Teye, E.; Qianqian, S.; Kwadzokpui, B.A.; Ekumah, J.-N.; et al. Flexible paper-based AuNP sensor for rapid detection of diabenz (a, h) anthracene (DbA) and benzo (b) fluoranthene (BbF) in mussels coupled with deep learning algorithms. *Food Control* **2025**, *168*, 110966. [CrossRef]
135. Huang, Y.; Li, Z.; Bian, Z.; Jin, H.; Zheng, G.; Hu, D.; Sun, Y.; Fan, C.; Xie, W.; Fang, H. Overview of deep learning and nondestructive detection technology for quality assessment of tomatoes. *Foods* **2025**, *14*, 286. [CrossRef] [PubMed]
136. Zhu, J.; Jiang, X.; Rong, Y.; Wei, W.; Wu, S.; Jiao, T.; Chen, Q. Label-free detection of trace level zearalenone in corn oil by surface-enhanced Raman spectroscopy (SERS) coupled with deep learning models. *Food Chem.* **2023**, *414*, 135705. [CrossRef]
137. Guo, Z.; Zhang, Y.; Xiao, H.; Jayan, H.; Majeed, U.; Ashiagbor, K.; Jiang, S.; Zou, X. Multi-sensor fusion and deep learning for batch monitoring and real-time warning of apple spoilage. *Food Control* **2025**, *172*, 111174. [CrossRef]
138. Mao, H.; Du, X.; Yan, Y.; Zhang, X.; Ma, G.; Wang, Y.; Liu, Y.; Wang, B.; Yang, X.; Shi, Q. Highly sensitive detection of daminozide using terahertz metamaterial sensors. *Int. J. Agric. Biol. Eng.* **2022**, *15*, 180–188. [CrossRef]
139. Lu, Y.; Asante, E.A.; Duan, H.; Hu, Y. Quantitative Assessment of Cold Injury in Tea Plants by Terahertz Spectroscopy Method. *Agronomy* **2023**, *13*, 1376. [CrossRef]
140. Gao, H.; Liu, Y.; Li, G.; Liu, H.; Shang, Y.; Ma, Z. On-demand design of terahertz metasurface sensors for detecting plant endogenous and exogenous molecules. *Agriculture* **2025**, *15*, 1481. [CrossRef]
141. Yu, J.; Pu, H.; Sun, D.-W. An advanced deep learning-driven Terahertz metamaterial sensor for distinguishing different red wines. *Chem. Eng. J.* **2025**, *504*, 158177. [CrossRef]
142. Tahir, H.E.; Arslan, M.; Mahunu, G.K.; Mariod, A.A.; Hashim, S.B.; Xiaobo, Z.; Jiyong, S.; El-Seedi, H.R.; Musa, T.H. The use of analytical techniques coupled with chemometrics for tracing the geographical origin of oils: A systematic review (2013–2020). *Food Chem.* **2022**, *366*, 130633. [CrossRef]
143. Zhang, X.; Wang, Y.; Zhou, Z.; Zhang, Y.; Wang, X. Detection method for tomato leaf mildew based on hyperspectral fusion terahertz technology. *Foods* **2023**, *12*, 535. [CrossRef]
144. Bonah, E.; Huang, X.; Aheto, J.H.; Osae, R. Application of hyperspectral imaging as a nondestructive technique for foodborne pathogen detection and characterization. *Foodborne Pathog. Dis.* **2019**, *16*, 712–722. [CrossRef]
145. Yang, Y.; Chai, F.; Huang, X.; Zhao, T.; Zhang, P.; Li, C.; Fang, B.; Hong, Z.; Yu, M.; Jing, X. Terahertz wave biomolecular sensor based on all-dielectric high Q metasurface. *Opt. Laser Technol.* **2024**, *169*, 110106. [CrossRef]
146. Song, S.-H.; Gao, Z.F.; Guo, X.; Chen, G.H. Aptamer-based detection methodology studies in food safety. *Food Anal. Methods* **2019**, *12*, 966–990. [CrossRef]
147. Ouyang, Q.; Wang, L.; Ahmad, W.; Yang, Y.; Chen, Q. Upconversion nanoprobes based on a horseradish peroxidase-regulated dual-mode strategy for the ultrasensitive detection of Staphylococcus aureus in meat. *J. Agric. Food Chem.* **2021**, *69*, 9947–9956. [CrossRef] [PubMed]
148. Ouyang, Q.; Rong, Y.; Wang, B.; Ahmad, W.; Liu, S.; Chen, Q. An innovative solid-phase biosensor for rapid on-site detection of N-nitrosodimethylamine incorporating zein film and upconversion nanoparticles. *Food Chem.* **2024**, *430*, 136981. [CrossRef]
149. Xu, Y.; Zhang, W.; Shi, J.; Li, Z.; Huang, X.; Zou, X.; Tan, W.; Zhang, X.; Hu, X.; Wang, X.; et al. Impedimetric aptasensor based on highly porous gold for sensitive detection of acetamiprid in fruits and vegetables. *Food Chem.* **2020**, *322*, 126762. [CrossRef]

Disclaimer/Publisher's Note: The statements, opinions and data contained in all publications are solely those of the individual author(s) and contributor(s) and not of MDPI and/or the editor(s). MDPI and/or the editor(s) disclaim responsibility for any injury to people or property resulting from any ideas, methods, instructions or products referred to in the content.